

AD-A053 612

**SUPERCONDUCTING ROTOR RESEARCH(U) GENERAL ELECTRIC
CORPORATE RESEARCH AND DEVELOPMENT SCHENECTADY N Y
B B GAMBLE ET AL. NOV 77 SRD-77-131 AFAPL-TR-77-68**

1/1

UNCLASSIFIED

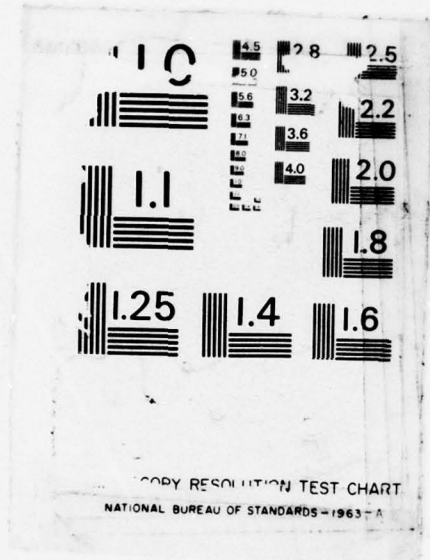
F33615-76-C-2167

F/G 9/7

NL

[Frame 1: Title page]	[Frame 2: Diagram]	[Frame 3: Diagram]	[Frame 4: Diagram]	[Frame 5: Diagram]	[Frame 6: Diagram]	[Frame 7: Diagram]	[Frame 8: Diagram]	[Frame 9: Diagram]	[Frame 10: Diagram]	[Frame 11: Diagram]	[Frame 12: Diagram]	[Frame 13: Diagram]	[Frame 14: Diagram]
[Frame 15: Diagram]	[Frame 16: Diagram]	[Frame 17: Diagram]	[Frame 18: Diagram]	[Frame 19: Diagram]	[Frame 20: Diagram]	[Frame 21: Diagram]	[Frame 22: Diagram]	[Frame 23: Diagram]	[Frame 24: Diagram]	[Frame 25: Diagram]	[Frame 26: Diagram]	[Frame 27: Diagram]	[Frame 28: Diagram]
[Frame 29: Diagram]	[Frame 30: Diagram]	[Frame 31: Diagram]	[Frame 32: Diagram]	[Frame 33: Diagram]	[Frame 34: Diagram]	[Frame 35: Diagram]	[Frame 36: Diagram]	[Frame 37: Diagram]	[Frame 38: Diagram]	[Frame 39: Diagram]	[Frame 40: Diagram]	[Frame 41: Diagram]	[Frame 42: Diagram]
[Frame 43: Diagram]	[Frame 44: Diagram]	[Frame 45: Diagram]	[Frame 46: Diagram]	[Frame 47: Diagram]	[Frame 48: Diagram]	[Frame 49: Diagram]	[Frame 50: Diagram]	[Frame 51: Diagram]	[Frame 52: Diagram]	[Frame 53: Diagram]	[Frame 54: Diagram]	[Frame 55: Diagram]	[Frame 56: Diagram]
[Frame 57: Diagram]	[Frame 58: Diagram]	[Frame 59: Diagram]	[Frame 60: Diagram]	[Frame 61: Diagram]	[Frame 62: Diagram]	[Frame 63: Diagram]	[Frame 64: Diagram]	[Frame 65: Diagram]	[Frame 66: Diagram]	[Frame 67: Diagram]	[Frame 68: Diagram]	[Frame 69: Diagram]	[Frame 70: Diagram]
[Frame 71: Diagram]	[Frame 72: Diagram]	[Frame 73: Diagram]	[Frame 74: Diagram]	[Frame 75: Diagram]	[Frame 76: Diagram]	[Frame 77: Diagram]	[Frame 78: Diagram]	[Frame 79: Diagram]	[Frame 80: Diagram]	[Frame 81: Diagram]	[Frame 82: Diagram]	[Frame 83: Diagram]	[Frame 84: Diagram]
[Frame 85: Diagram]	[Frame 86: Diagram]	[Frame 87: Diagram]	[Frame 88: Diagram]	[Frame 89: Diagram]	[Frame 90: Diagram]	[Frame 91: Diagram]	[Frame 92: Diagram]	[Frame 93: Diagram]	[Frame 94: Diagram]	[Frame 95: Diagram]	[Frame 96: Diagram]	[Frame 97: Diagram]	[Frame 98: Diagram]
[Frame 99: Diagram]	[Frame 100: Diagram]	[Frame 101: Diagram]	[Frame 102: Diagram]	[Frame 103: Diagram]	[Frame 104: Diagram]	[Frame 105: Diagram]	[Frame 106: Diagram]	[Frame 107: Diagram]	[Frame 108: Diagram]	[Frame 109: Diagram]	[Frame 110: Diagram]	[Frame 111: Diagram]	[Frame 112: Diagram]
[Frame 113: Diagram]	[Frame 114: Diagram]	[Frame 115: Diagram]	[Frame 116: Diagram]	[Frame 117: Diagram]	[Frame 118: Diagram]	[Frame 119: Diagram]	[Frame 120: Diagram]	[Frame 121: Diagram]	[Frame 122: Diagram]	[Frame 123: Diagram]	[Frame 124: Diagram]	[Frame 125: Diagram]	[Frame 126: Diagram]
[Frame 127: Diagram]	[Frame 128: Diagram]	[Frame 129: Diagram]	[Frame 130: Diagram]	[Frame 131: Diagram]	[Frame 132: Diagram]	[Frame 133: Diagram]	[Frame 134: Diagram]	[Frame 135: Diagram]	[Frame 136: Diagram]	[Frame 137: Diagram]	[Frame 138: Diagram]	[Frame 139: Diagram]	[Frame 140: Diagram]
[Frame 141: Diagram]	[Frame 142: Diagram]	[Frame 143: Diagram]	[Frame 144: Diagram]	[Frame 145: Diagram]	[Frame 146: Diagram]	[Frame 147: Diagram]	[Frame 148: Diagram]	[Frame 149: Diagram]	[Frame 150: Diagram]	[Frame 151: Diagram]	[Frame 152: Diagram]	[Frame 153: Diagram]	[Frame 154: Diagram]

END
DATE
FILMED
DTIC
JULY 88



COPY RESOLUTION TEST CHART
NATIONAL BUREAU OF STANDARDS - 1963 - A

AFAPL-TR-77-68

2H

AD A 053612

SUPERCONDUCTING ROTOR RESEARCH

Corporate Research and Development
General Electric Company
Schenectady, New York 12301

DDC
MAY 8 1978
F

AD NO. ~~1~~
DDC FILE COPY

November 1977

Phase I Interim Technical Report

1 November 1976 - 31 July 1977

Approved for public release; distribution unlimited.

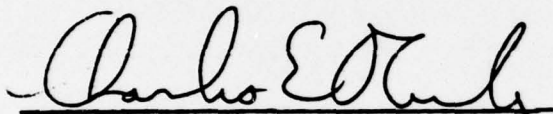
AIR FORCE AERO PROPULSION LABORATORY
AIR FORCE WRIGHT AERONAUTICAL LABORATORIES
AIR FORCE SYSTEMS COMMAND
WRIGHT-PATTERSON AIR FORCE BASE, OHIO 45433

NOTICE

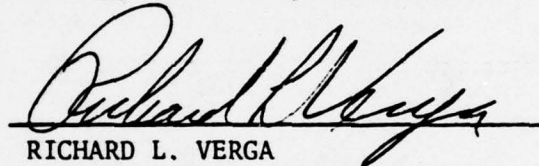
When Government drawings, specifications, or other data are used for any purpose other than in connection with a definitely related Government procurement operation, the United States Government thereby incurs no responsibility nor any obligation whatsoever; and the fact that the government may have formulated, furnished, or in any way supplied the said drawings, specifications, or other data, is not to be regarded by implication or otherwise as in any manner licensing the holder or any other person or corporation, or conveying any rights or permission to manufacture, use, or sell any patented invention that may in any way be related thereto.

This report has been reviewed by the Information Office (OI) and is releasable to the National Technical Information Service (NTIS). At NTIS, it will be available to the general public, including foreign nations.

This technical report has been reviewed and is approved for publication.

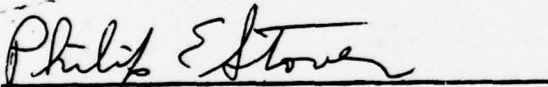


CHARLES E. OBERLY
Project Engineer
High Power Branch
Aerospace Power Division



RICHARD L. VERGA
TAM, High Power Branch
Aerospace Power Division

FOR THE COMMANDER



PHILIP E. STOVER
Chief, High Power Branch
Aerospace Power Division

"If your address has changed, if you wish to be removed from our mailing list, or if the addressee is no longer employed by your organization please notify AFAPL/POD-1, W-PAFB, OH 45433 to help us maintain a current mailing list".

Copies of this report should not be returned unless return is required by security considerations, contractual obligations, or notice on a specific document.

UNCLASSIFIED

SECURITY CLASSIFICATION OF THIS PAGE (When Data Entered)

19 REPORT DOCUMENTATION PAGE		READ INSTRUCTIONS BEFORE COMPLETING FORM
18 1 REPORT NUMBER AFAPL-TR-77-68 ✓	2. GOVT ACCESSION NO.	3. RECIPIENT'S CATALOG NUMBER 9
6 4 5 6 7 8 9 10 11 12 13 14 15 16 17 18 19 20 21 22 23 24 25 26 27 28 29 30 31 32 33 34 35 36 37 38 39 40 41 42 43 44 45 46 47 48 49 50 51 52 53 54 55 56 57 58 59 60 61 62 63 64 65 66 67 68 69 70 71 72 73 74 75 76 77 78 79 80 81 82 83 84 85 86 87 88 89 90 91 92 93 94 95 96 97 98 99 100		5. TYPE OF REPORT & PERIOD COVERED Phase I Interim Technical Report 1 Nov 76 - 31 Jul 77
6. AUTHOR(s) B. B. Gamble, T. A. Keim and P. A. Rios		7. PERFORMING ORG. REPORT NUMBER SRD-77-131 ✓ <i>on Phase I</i>
9. PERFORMING ORGANIZATION NAME AND ADDRESS Corporate Research and Development General Electric Company Schenectady, New York 12301		8. CONTRACT OR GRANT NUMBER(s) F33615-76-C-2167 <i>NEW</i>
11. CONTROLLING OFFICE NAME AND ADDRESS Air Force Aero Propulsion Laboratory (POD) Wright-Patterson Air Force Base, Ohio 45433		10. PROGRAM ELEMENT, PROJECT, TASK AREA & WORK UNIT NUMBERS Project 3145-32-44
14. MONITORING AGENCY NAME & ADDRESS (if different from Controlling Office) 12 89p.		12. REPORT DATE November 1977
16. DISTRIBUTION STATEMENT (of this Report) Approved for public release, distribution unlimited		13. NUMBER OF PAGES 95
17. DISTRIBUTION STATEMENT (of the abstract entered in Block 20, if different from Report)		15. SECURITY CLASS. (of this report) Unclassified
18. SUPPLEMENTARY NOTES		15a. DECLASSIFICATION/DOWNGRADING SCHEDULE
19. KEY WORDS (Continue on reverse side if necessary and identify by block number) cryogenics, superconductivity, synchronous generators		
20. ABSTRACT (Continue on reverse side if necessary and identify by block number) This report summarizes work completed for the Air Force Aero Propulsion Laboratory in Phase I of a program entitled Superconducting Rotor Research. The objective of this program is to incorporate new materials in the design of an airborne, 20 MW, high-speed, superconducting generator. The rotor of the generator will be constructed and its current density demonstrated. The Phase I work consisted of a sizing study to select the machine configuration and dimensions, a survey of superconducting materials, and selection of the superconductor for this application.		

DDC
MAY 3 1978
F

406627

JP

FOREWORD

This interim technical report covers Phase I development work performed under Contract F33615-76-C-2167 with the Department of the Air Force, Air Force Systems Command, Air Force Aero Propulsion Laboratory, Wright-Patterson Air Force Base, Ohio. The work was performed in the Power Generation and Propulsion Laboratory of Corporate Research and Development at the General Electric Company in Schenectady, New York. Work described herein covers the period from 1 November 1976 to 31 July 1977. Work was initiated 1 November 1976 under Project 3145.

The program was under the direction of C. Oberly of the Aero Propulsion Laboratory; this report was submitted in August 1977.

The General Electric program manager was P. A. Rios, and the report was authored by the principal contributors to the program:

P. A. Rios
T. A. Keim
B. B. Gamble

ACCESSION for	
NTIS	Write Section <input checked="" type="checkbox"/>
DDC	B. ft Section <input type="checkbox"/>
UNANNOUNCED	<input type="checkbox"/>
JUSTIFICATION _____	
BY	
DISTRIBUTION/AVAILABILITY CODES	
Dist	SP. CIAL
A	

Blank
14

TABLE OF CONTENTS

<u>Section</u>	<u>Page</u>
I INTRODUCTION AND SUMMARY	1
Contract Objectives	1
Design Requirements	1
Phase I Results	2
Summary	4
II SIZING STUDY	5
Purpose	5
Machine Configurations	5
Parametric Studies	6
Sensitivity Considerations	7
Selected Base Designs	13
III FIELD DISTRIBUTION AND BASE WINDING DESIGNS	15
Base Designs	15
Analysis	16
Field Distribution	17
In the Modules	17
In the Armature	20
Effect of Field Distribution on Sizing Study Results	20
IV SUPPORT SYSTEM	25
Design Considerations	25
Support System Configurations	26
Analysis	28
Summary	31
V ELECTROMAGNETIC SHIELD	33
Function and Requirements	33
Adequate Magnetic Field Attenuation vs Frequency	33
Adequate Torsional Strength	33
Adequate Strength for Crushing Load	34
Acceptable Natural Frequencies	34
Material and Thickness Selection	34
Shielding Requirements	35
Considerations of Crushing Load	36
Shield Vibration	37
Summary	38
VI SUPERCONDUCTOR SURVEY	39
Introduction	39
Results	39
Survey Results as Applied to the Base Design	40
Cabled Superconductors	42

TABLE OF CONTENTS (CONT'D)

<u>Section</u>	<u>Page</u>
VII FIELD RAMPING	45
Introduction	45
Coil Composite Properties	45
Results	46
Aspected Conductors	47
Ramping Voltage	48
VIII QUENCH PROTECTION	49
Introduction	49
Simple Protection Circuit	49
Alternate Protection Systems.	51
IX ROTOR COMPONENT WEIGHTS AND SUPERCONDUCTOR PERFORMANCE	53
X RECOMMENDED SUPERCONDUCTOR MEASUREMENTS	55
Recommended Measurements.	55
Cable Impregnation	56
XI SUPERCONDUCTOR SELECTION.	59
Superconductor Requirements	59
Preferred Conductor Specification	59
Preferred Monolithic Conductor Specification.	61
XII CONCLUSIONS.	63
Appendix A SUPERCONDUCTOR REQUIREMENTS	65
Appendix B SUPERCONDUCTOR SURVEY	69
REFERENCES	87

LIST OF ILLUSTRATIONS

<u>Figure</u>	<u>Page</u>
1 Four-Pole Winding Geometry	10
2 Flux Linkage Schematic Diagram	11
3 Eight-Pole Winding Geometry.	12
4 Winding Configuration	16
5 Module Configuration	17

LIST OF ILLUSTRATIONS (CONT'D)

<u>Figure</u>		<u>Page</u>
6	Flux Density Distribution in Section A	18
7	Flux Density Distribution in Section B	18
8	Flux Density Distribution in Section C	19
9	Flux Density Distribution in Section D	19
10	Field Orientation (Section B)	20
11	Comparison Between the Least-Squares-Fit, Two-Dimensional Model and Biot-Savart Law Radial Component of Magnetic Flux Density at $r = 10.5$ Inches	21
12	Comparison Between the Least-Squares-Fit, Two-Dimensional Model and Biot-Savart Radial Component of Magnetic Flux Density at $r = 11.5$ Inches	21
13	Comparison of Racetrack Modules and Annular-Sector Representation	22
14	Winding Loading	25
15	Support System Design Concept	27
16	Winding and Support System Finite-Element Representation (Composite Torque Tube).	29
17	Winding and Support System Finite Element Representation (Metallic Torque Tube).	30
18	Conductor Spacing	46
19	Temperature Distribution Following a One-Second Field Ramp.	46
20	Field Orientation for an Aspected Conductor	47
21	Nodal Representation and Module Temperature Distribution Following an Assumed Quench (with a Protection Circuit)	50
22	Parallel Module Winding	51
23	Cylindrical Module Geometry	56
24	Cylindrical-Module Field Distribution	57
25	Preferred Cable Configuration	60
26	Core Current Density	61
27	Preferred Monolithic Configuration	62

LIST OF TABLES

<u>Table</u>		<u>Page</u>
1	Minimum Weight in Pounds for Several Machine Concepts	7
2	Comparison of Configurations	8
3	Weight Sensitivity.	12
4	Base Designs	15
5	Revised Base Design—Concentric End Turn.	23
6	Support Structure Materials	27
7	Torque Tube Materials.	27
8	Superconductor Survey	39
9	Base Design Superconductor Comparison	41
10	Rotor Component Weight Estimates	53
11	Recommended Additional Measurements of Nb ₃ Sn Properties	55
12	Preferred Conductors	62
B.1	Conductor A	71
B.2	Conductor A'	72
B.3	Conductor B	73
B.4	Conductor B'	74
B.5	Conductor C	75
B.6	Conductor D	76
B.7	Conductor E	77
B.8	Airco Conductor A	78
B.9	Airco Conductor B	79
B.10	Airco Conductor C	80
B.11	Airco Conductor D	81
B.12	Supercon.	82
B.13	Hisuper 331; ZF-120B	83
B.14	Hisuper 331; CF-96B	84
B.15	Toshiba	85

Section I

INTRODUCTION AND SUMMARY

CONTRACT OBJECTIVES

The objective of this contract is to incorporate new techniques and materials in the design of an airborne, 20 MW, high-speed superconducting generator. The rotor for the generator will be constructed, and the high current density capability of the rotor will be demonstrated in a stationary test, under steady state and field ramping conditions. The contract includes the following four phases:

- Phase I - Superconducting Materials Selection
- Phase II - Generator Design
- Phase III - Rotor Fabrication
- Phase IV - Rotor Test

The Phase I effort, directed toward the selection of a superconducting material, included the following tasks:

- A survey of superconducting materials available from superconductor manufacturers.
- Calculation of the impact that the superconductor characteristics have on the predicted performance of the generator.
- Recommendation of additional properties measurements needed for evaluation of the superconductor.
- Final selection of a superconductor to be used for the generator design of Phase II.

DESIGN REQUIREMENTS

The following are the design requirements for the generator:

- Output: 20 MW
- Voltage: 20 to 40 kV (from rectifier)
- Rpm: 5500 to 6800 (6000 nominal selected for Phase I)
- Moment of Inertia: 10 slug-ft²
- Rotor Tip Speed: 500 ft/sec
- Ramping Rate: 1 second to full field current
- Torsional Acceleration: 1 second to full speed

- Specific Weight: 0.1 lb/kW
- Run Time: 5 minutes continuous or pulsed

PHASE I RESULTS

The development of the advanced superconducting rotor for use in an air-borne power system began with a sizing study to determine the preferred generator configuration. This sizing study approximately modeled generators with 1 through 6 pole pairs. Involute, toroidal, and concentric stator end turns were considered with iron and conductive environmental shields. On the basis of this study, four-pole generators with conductively shielded stators were selected as base designs. Both involute and concentric end turns were considered.

The analysis indicated these machines have the potential for meeting the weight requirement of 0.1 lb/kW. A sensitivity analysis indicated these machines were the least sensitive to inaccuracies in the approximate analysis, thus providing the flexibility necessary for further design modification.

Dimensions for a field winding utilizing racetrack-shaped modules were tentatively selected for the base designs. The field distribution generated by this base design winding was calculated. This field distribution is necessarily less effective in producing power than that of the annular-sector model assumed in the sizing study. A revised base design of increased active length to allow for this difference has been developed for the concentric-end-turn generator.

Tentative field-winding support systems were investigated to determine the adequacy of the rotor design. A finite element analysis indicated two potential support systems are feasible.

Rectified load effects and shielding requirements were also investigated. The results indicate the rotor can be effectively shielded (within the revised base-design space requirement) from the 5th and 7th harmonics resulting from the rectified loading. Shield vibration has been identified as a design consideration deserving detailed analysis in the next phase.

The selection of a superconductor is best accomplished as an integral part of the superconducting generator design. This has been accomplished to a degree through the use of a sizing study and sensitivity analysis to define preferred base designs. Unfortunately, this work was completed only after the superconductor survey requests had been mailed. The definition of the requirements for the survey therefore do not completely reflect the results of the generator analysis. It is felt that this did not significantly impact the results of the superconductor survey. The generator analysis has been utilized to select from among the superconductors proposed in the survey.

During Phase I, there was significant interaction with superconductor manufacturers. In particular, the Intermagnetics General Corporation and Airco Inc. were both visited for the purpose of discussing the requirements. Superconductor properties measurements were suggested to both of these manufacturers.

It has been assumed in the selection of a superconductor that the impregnation and winding processes utilized at General Electric in the manufacture of racetrack windings for the General Electric 20 MVA superconducting generator rotor would be utilized in the Advanced Superconducting Rotor. This impregnation process is a well proven method for restricting wire motion which manifests itself as the phenomenon called "training."

The design goal which impacts most strongly on superconductor selection is the ramp of the field-winding current to operating level in one second. In designing to meet this goal, a winding is required which has substantially more temperature margin than would be designed for steady-state operation. The winding is therefore designed on the basis of its transient performance. A superconductor must be selected which has sufficient temperature margin (or enthalpy margin) at the steady-state operating condition to allow the losses incurred by ramping in one second to the operating current to be absorbed without a normal transition. This requirement favors the use of a Nb_3Sn superconductor over a $NbTi$ superconductor.

The ramping of the base design winding was investigated with a transient heat transfer computer program. Aspected conductors were investigated, and it was determined that the dependence of the losses on field orientation precludes the selection of a highly aspected conductor.

The base-design winding was analyzed for protection requirements. A protection circuit was found to be required to allow rapid dissipation of the rotor winding's stored energy in an external resistor in the event of a quench. The results determine the downward ramping rate required to protect the winding. This requirement favors the selection of a high-current conductor, while losses and bend radius favor the selection of a low-current conductor.

A cabled superconductor combines the desirable features of low ramping losses and small minimum bend radius in large current sizes. Development of the impregnation process for a cabled superconductor is planned as part of the U. S. Air Force funded materials development program at IGC. Manufacture and test of a coil that is representative of a field-winding module is recommended in addition to the currently planned development.

An alternate superconductor has been selected in the event that the impregnation difficulties cannot be overcome for cabled superconductors. A slightly aspected monolithic conductor can be used if the winding modules are connected in parallel. Connection in parallel reduces the voltage required to achieve a given ramping rate. However, equal current sharing among the modules for steady-state and transient operation must be ensured.

SUMMARY

- Four-pole generators with stators that utilize involute and concentric end turns were selected as base designs.
- Racetrack-shaped epoxy-impregnated modules were selected and fields, ramping, and quenching were analyzed.
- The base design was revised to reflect the field distribution generated by the racetrack-shaped modules.
- Shielding and winding support was determined to be feasible within the constraints of the base design.
- Shield vibration was identified as a major design consideration.
- A cabled Nb_3Sn superconductor was selected contingent on impregnation development.
- A slightly aspected Nb_3Sn superconductor was selected as an alternate conductor for use in a winding with the modules connected in parallel.

Section II

SIZING STUDY

PURPOSE

The generator which is to be designed in this program is different in several respects from any device in existence. The principal requirement that makes this generator different is of course the rapid start, which can be met only with a rotor conductor carefully selected from among the best available. Proper selection of the conductor was the principal objective of the Phase I work. Conductor influence on generator design is an important consideration in conductor selection, so a means to evaluate this influence is a useful contribution to the selection task. Furthermore, many aspects of conductor performance can best be evaluated within the context of a specific field winding design. The design chosen for these purposes should be reasonably representative of that which will ultimately be selected. To evaluate conductor influence on design, and to help in selecting a typical base design, a general sizing study has been performed.

MACHINE CONFIGURATIONS

In addition to one-second startup requirement, other specifications of the generator are unlike those of any other superconducting generator. In general, the lightest machine with the requisite output and startup capability is sought. Mechanical speed is fixed at a nominal 6000 rpm; the rectifier load permits free selection of output frequency. The desired output voltage (20 or 40 kV at the dc side of the rectifier) is higher than that which is natural for the power rating.

The high voltage requirement suggests consideration of winding configurations which are amenable to construction with conductor insulation adequate only for turn-to-turn voltage. The conventional involute-end-turn, slotless construction can be built with only turn-to-turn insulation within straight portions of the phase belts, although more insulation is required between end turns.¹ In any case, the involute end-turn configuration merits consideration, if for no other purpose than to provide a familiar base case for comparisons. A second configuration, which has recently received considerable attention for high-voltage applications, is the toroidally wound armature,² in which the current returns axially outside the iron core. The applicability of this construction to the present case deserves investigation. Finally, concentric reentrant end turns³ permit the turns of a phase belt to be kept together and insulated as a unit both in the straight section and in the end turns. This configuration should also be considered.

It has long been recognized that the fundamental field-terminating function of the iron core in a superconducting generator can be performed by a sufficiently

conductive metallic case. Conductively shielded generators typically offer lower weight at the expense of increased losses and volume.

In view of the prime importance of weight in the present application, conductive stator shields deserve careful attention.

A minimum-weight machine of this speed and rating will tend to have a relatively low length-to-diameter ratio. The end turns will comprise a significant part of the total armature weight, so differences in end-turn configuration may be significant to the overall machine weight. The end-turn contribution will scale differently with the number of poles for different configurations. To make a realistic comparison among configurations, a parametric optimization study must be performed for each candidate configuration. The final design can then be selected from among the best of each configuration.

PARAMETRIC STUDIES

Parametric studies have been performed for each of five configurations: involute end turns and concentric end turns (each with both iron and conductive shields) and the toroidal armature with iron yoke and conductive shield. (A toroidal armature with no iron yoke is theoretically possible, but this configuration has not been studied in detail.) Rating and reactance expressions were developed from the two-dimensional annular-sector model⁴ corrected for finite length by quasi-empirical or intuitive but conservative factors. Weight estimates included only field and armature conductors and whatever iron or conductive (aluminum) shields may be required.

For each configuration the field-winding outside radius, field-winding thickness, armature thickness, shield inside radius, and number of poles were each varied over a range. For each set of dimensions, the length required to achieve rating and the corresponding weight were computed. Current density in both field and armature windings was held constant in all cases, as was the gap between field and armature and the fraction of the field-winding annulus occupied by pole-face material. Table 1 shows the weight of the lightest machine of each configuration, for each of several numbers of poles.

The approximations made to arrive at Table 1 are of necessity coarse, so it would be an error to select the preferred configuration on the basis of this information alone. Several broad conclusions are probably justified. The toroidal armature suffers from a severe weight penalty. Iron-shield designs have a weight minimum in the eight-pole configuration; with conductive shields, the minimum is nearer six poles. Weight differences between involute and concentric end turns are of little consequence. Four-pole through ten-pole conductively shielded machines and six-pole through ten-pole iron-shielded machines may be considered to have the potential for acceptable weight.

Table 1

MINIMUM WEIGHT IN POUNDS FOR SEVERAL MACHINE CONCEPTS
20 MW, 0.9 Power Factor

Configuration	Number of Poles				
	4	6	8	10	12
Conductive Shield, Involute end turns	916	859	912	1120	1450
Conductive Shield, Concentric end turns	954	-	903	-	1400
Iron Shield, Concentric end turns	1670	-	990	-	1320
Iron Shield, Involute end turns	1610	1130	1000	1120	1340
Toroidal Armature	1990	1570	1400	1530	1690

CE 266

Table 2 compares in more detail the dimensions and parameters of the minimum-weight machines in each of these configurations. Again, because of the approximate nature of the results, only broad generalizations are appropriate; detailed conclusions may be inaccurate. The largest field-winding radius considered produces minimum-weight configurations. The search was stopped at 9 inches to limit tip speed, and thus mechanical stresses, to manageable levels. A two-inch-thick field winding seems preferable to a three-inch-thick winding. Similarly, a two-inch-thick armature winding is generally indicated. If an iron shield is used, it should be at a large radius; 20.5 inches was the largest considered. The weight saving due to reduced thickness of the shield more than makes up for the weight penalty due to increased length of all the active components.

The two four-pole entries have one-inch armature thicknesses and a correspondingly low synchronous reactance, but it is likely that a study with finer steps in armature thickness would show a more continuous transition to thinner armatures and lower reactances; hence, for present purposes, the step change is of little significance. With this observation in mind, there are no differences in Table 2 of sufficient importance to warrant elimination of any possibilities.

SENSITIVITY CONSIDERATIONS

The use of approximate expressions for weight and magnetic equivalent length and of fixed values for current densities and gap was an expedient essential to the timely completion of a sizing study. The resulting inaccuracy need not be an extreme handicap if it is possible to consider the

Table 2
COMPARISON OF CONFIGURATIONS

Number of Poles	Type Code	R1	R2	R3	R4	L	RS	WCU	WSC	WFE	WAL	XD	BMAX	WT
4	CI	7	9	10.5	11.5	10.8	17.3	241	377	-	297	0.074	4.4	916
4	CC	7	9	10.5	11.5	13.5	17.3	210	421	-	323	0.083	4.4	954
6	CI	7	9	10.5	12.5	9.1	15.6	392	286	-	181	0.24	4.3	859
6	II	7	9	10.5	12.5	6.8	20.5	359	248	278	243	0.27	4.4	1139
8	CI	7	9	10.5	12.5	14.4	15.6	406	338	-	168	0.31	4.1	912
8	CC	7	9	10.5	12.5	16.2	15.6	363	367	-	173	0.31	4.1	903
8	IC	7	9	10.5	12.5	14.4	20.5	337	338	142	172	0.33	4.2	990
8	II	7	9	10.5	12.5	12.8	20.5	384	312	129	180	0.33	4.2	1000
10	CI	7	9	10.5	12.5	22.8	15.6	487	452	-	180	0.41	3.9	1120
10	II	6	9	10.5	12.5	12.3	12.5	342	391	328	63	0.46	5.1	1120

CODE

- CI Conductive shield involute end turns WCU Weight of armature copper, lb
 CC Conductive shield concentric end turns WSC Weight of superconductor, lb
 II Iron shield involute end turns WFE Weight of iron shield, lb
 IC Iron shield concentric end turns WAL Weight of aluminum shield (if any) plus weight of aluminum end shields, lb
 R1 Field winding inside radius, inches XD Synchronous reactance, per unit
 R2 Field winding outside radius, inches BMAX Amplitude of field-winding fundamental flux density, tesla
 R3 Armature winding inside radius, inches WT Weight, lb
 R4 Armature winding outside radius, inches
 RS Shield inside radius, inches
 L Straight section length, inches

sensitivity of the results to the assumptions when evaluating the outcome. A semiquantitative assessment of this sensitivity can be accomplished without a great deal of difficulty.

Errors in the parametric study can be associated with several distinct causes:

- Errors in the weight expressions
- Errors in the magnetic equivalent lengths
- Differences between the annular sector winding cross sections assumed by the magnetic field model and the winding cross sections actually achieved
- Differences between assumed and achievable values of the fixed parameters

Of these sources of error, the first is probably the least significant. The geometry of the armature winding can be fairly precisely defined, as can its mean density. An iron shield is a simple hollow cylinder, the thickness of which is readily determined by the requirement to keep flux density in the iron below the saturation level. The iron shield is presumed to project halfway over the end turns. Iron-shielded machines (not including toroidally wound armatures) have a weight allowance for aluminum end-turn shields extending cylindrically out from the end of the iron to the end of the end turns. The remaining configurations include an aluminum shield over the entire length of the armature. In all cases, aluminum annular plates are provided to shield axial flux. The thickness of all aluminum shields is three skin depths at fundamental frequency. In applications where aluminum weight is significant, the necessity of this thickness may be reexamined.

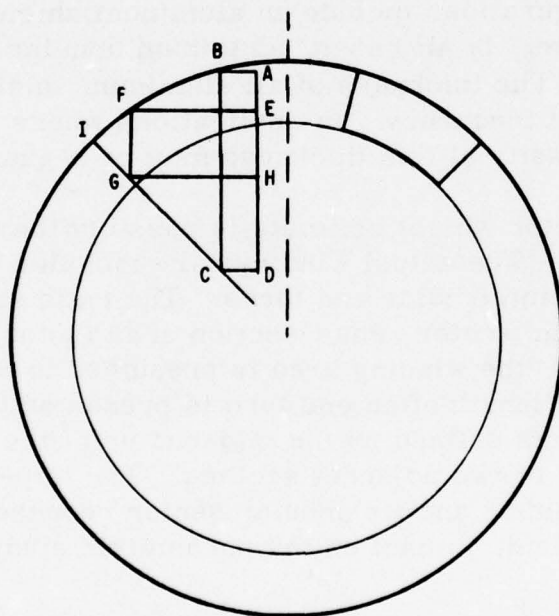
The superconductor weight estimate is possibly the largest contributor to total weight error. The actual windings are modules with rectangular cross sections and semicircular end turns. The ratio of module cross-section area to annular sector cross-section area is not readily determined. For weight estimates, the winding area is presumed to be that of the annular sector, and the mean length of an end turn is presumed to be that of a semicircle connecting points defined by the mid-radius of the winding annulus and the angular bisectors of two adjacent sectors. The imperfect equivalence between a racetrack winding and its annular sector representation has a second, possibly more important, impact on the parametric study, which will be discussed shortly.

Three-dimensional magnetic-field solutions by digital computer are only beginning to be applied to superconducting generator designs. The only other accurate technique that has been applied to the study of end effects in superconducting generators is scale-model testing. Even when these techniques

are available, their cost is such that their use is typically confined to verifying or correcting the terms by which the physical winding lengths have been modified for use in equations derived from two-dimensional models. For most of the configurations under study, no three-dimensional information is available.

In the absence of such data, no quantitative assessment of error is possible, but some appreciation of the magnitude for potential error can be obtained by comparing physical end-turn dimensions to the straight length. The total end-turn correction is on the order of the axial projection of an end turn at most; the error should be some fraction of the correction. Long machines with short end turns are less sensitive to errors in magnetic equivalent length.

The geometric difference between a racetrack module and the annular-sector winding used to represent it for analytical purposes has already been discussed in the context of weight estimation. The difference between the two from the standpoint of magnetic performance can be understood by reference to Figure 1. The right half of the figure shows the annular sector attributed to one side of the winding for one pole of a four-pole winding. The left half shows two possible rectangular cross sections of equivalent area: rectangles ABCDA and EFGHE. Any number of other rectangles are possible within the area ABFGCDHEA. The boundary AEHD is set by the minimum bend radius of the superconductor; line IGC is a boundary imposed by symmetry.



4 POLES

9 INCH OUTSIDE RADIUS

7 INCH INSIDE RADIUS

Figure 1. Four-Pole Winding Geometry

To compare the flux linkage with the armature due to the annular sector with the flux linkage due to a rectangular cross section, consider the situation in Figure 2. The flux linkage with coil A-A' generated by the element of current which enters the paper at Point I and returns at Point I' increases as the location of Point I moves radially outward and also as the location moves tangentially away from the vertical line marking the axis of the figure.

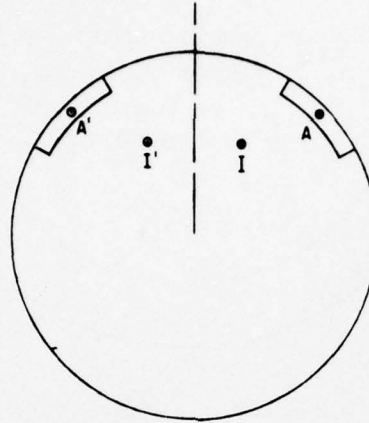
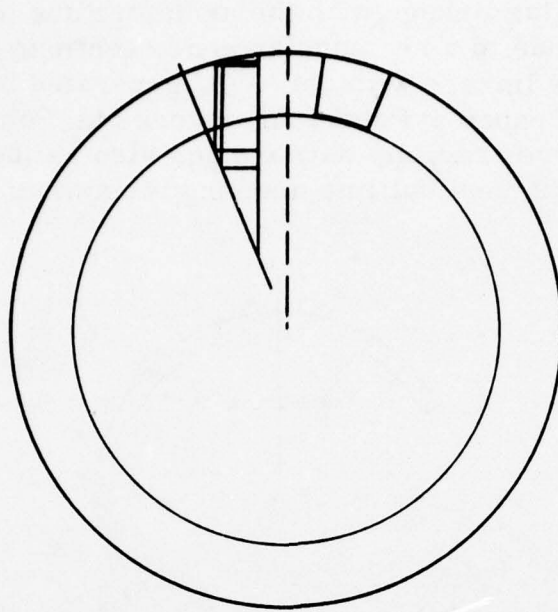


Figure 2. Flux Linkage Schematic Diagram

Reference to Figure 1 shows that the annular sector places the current elements in locations where they generate relatively high mutual flux. If the transition to a rectangle is considered to be the motion of current elements from points outside to points inside the rectangle, it can be seen that the rectangle will generate less mutual flux. The mutual flux can be increased by selecting a rectangular cross section with larger area, but only at the expense of increased winding weight. The extent to which winding cross section can be increased diminishes as the number of poles increases. Figure 3 shows that for an eight-pole winding the size and shape of the racetrack module are not free to vary significantly.

The sensitivity of the model to changes in field location and to values of the fixed parameters can be determined by a fairly straightforward procedure. Starting with a reasonable base case, the value of one of the parameters, V_n , is changed by a small amount; all other parameters are held constant. The straight section length is recomputed to keep output constant, and the percentage change in weight divided by the percentage change in the parameter V_n is computed. The result may be called the sensitivity of weight with respect to V_n . Table 3 shows the sensitivity of weight to each of six parameters for conductively shielded involute machines with four poles and eight poles.

The desirability of low or high sensitivity with respect to a parameter depends on the sign of the expected error in that parameter. The direction in which the weight will vary in response to an increase in the parameter determines the sign of the sensitivity. If the expected change in the parameter in



8 POLES
 9 INCH OUTSIDE RADIUS
 7 INCH INSIDE RADIUS

Figure 3. Eight-Pole Winding Geometry

Table 3
 WEIGHT SENSITIVITY

Parameter Varied, V	Base Value	Weight Sensitivity	Length Sensitivity
4 Poles			
Field thickness	2 in.	0.063	-0.50
Armature thickness	1 in.	0.052	-0.53
Field radius	9 in.	-0.32	-4.5
Gap	1.5 in.	0.22	0.20
Field current density	15,000 A/cm ²	-0.79	-1.7
Armature current density	600 A/cm ²	-0.79	-1.8
8 Poles			
Field thickness	2 in.	0.060	-0.33
Armature thickness	2 in.	0.33	-0.31
Field radius	9 in.	-1.5	-4.7
Gap	1.5 in.	0.47	0.56
Field current density	15,000 A/cm ²	-1.1	-1.7
Armature current density	600 A/cm ²	-0.77	-1.2

going from assumed to achieved value is in such a direction as to increase weight, a low absolute value of sensitivity is desired and vice versa.

Conversion of an annular sector to an equivalent-area racetrack can be considered to be similar to a reduction in field radius and an increase in gap. Both effects act to increase weight, so low absolute values are desirable. The four-pole configuration suffers less from this error.

The values for the winding current densities and gap dimension which were used for the sizing study were selected as achievable but ambitious. Any deviations in the final machine are likely to be in the direction of increased weight. Again, the four-pole configuration is preferable. The small sensitivities with respect to armature thickness are not surprising. The base case has been optimized with respect to these dimensions; therefore, if the optimization and the sensitivity computation had both been performed carefully enough, the answer could have been expected to be zero.

SELECTED BASE DESIGNS

The four-pole conductively shielded configurations with both involute and concentric end turns have been chosen as base cases for computations pertaining to superconductor selection. The sensitivity arguments favor four poles. Four-pole machines can be expected to be simpler to design and construct, requiring fewer pieces and fewer fabrication operations. Arguments for four poles are essentially arguments for conductive shielding; the four-pole iron-shielded configurations are at an intolerable weight disadvantage.

A comparison of the best conductively shielded and iron-shielded machines shows no tremendous construction advantage or shielding superiority for the machines with iron. The optimum location for the iron shield is 8 inches away from the back of the armature, or perhaps even farther away; no larger separations were considered. With the shield so far removed from the armature, mechanical support of the armature is little different than for a conductive-shield configuration. Since the field enhancement due to the shield is small, the lengths of the two machines are not substantially different, and the conductively shielded machine tends to optimize at smaller shield radius and smaller total volume.

With the iron shield at a high radius, there is a large axial area for flux paths which do not reach the shield. This flux will probably be controlled with conductive shielding, and as a result, the machine will exhibit magnetic field leakage vs speed characteristics not unlike a totally conductively shielded device. There appears to be no advantage to iron-shielded construction to counter the weight disadvantage; therefore a four-pole conductively shielded device was selected.

No argument has been advanced to favor either of the two candidate end-turn arrangements. But the difference between the two field windings is only

a small difference in straight length; so for present purposes there is no overwhelming need to select between them.

The only disadvantage of this selection is the low (probably unrealistically low) reactances resulting from the thin armature. More careful weight optimization in Phase II may well lead to selection of a thicker armature and higher reactances. If this does not occur, and if higher reactances are desired (e. g., to limit fault currents), the low weight sensitivity to armature thickness will make it possible to achieve a higher-reactance design with little weight penalty.

Section III

FIELD DISTRIBUTION AND BASE WINDING DESIGNS

BASE DESIGNS

The process of selecting a superconductor for the rotor field winding must involve a reference to a particular winding design. Different designs will by nature of their requirements dictate the selection of different superconductors. Several characteristics of the winding under consideration have particularly strong effects on superconductor selection. The field distribution is particularly important in that the winding is to be designed with the goal of a one-second ramp to full field current, and the minimum bend radius impacts on the conductor design, which in turn affects the transient performance for a given field distribution.

For the purpose of comparing superconductors it is necessary to select a preliminary winding configuration. Winding design is an iterative process, and the details of the selected base designs will be optimized for the selected superconductor during Phase II.

The parametric studies described in the previous section have identified conductively shielded machines as potentially the lightest for the application under investigation. The significant parameters for the four-pole generators with involute and concentric wound armatures are presented in Table 4.

Table 4
BASE DESIGNS

<u>Parameter</u>	<u>Conductively Shielded</u>	
	<u>Involute</u>	<u>Concentric</u>
Field Winding Current Density (A/cm ²)	15,000	15,000
Stator Winding Current Density (A/cm ²)	600	600
Inside Radius of Field Winding (in.)	7	7
Outside Radius of Field Winding (in.)	9	9
Inside Radius of Stator Winding (in.)	10.5	10.5
Outside Radius of Stator Winding (in.)	11.5	11.5
Conductive Yoke Radius (in.)	17.3	17.3
Active Length (in.)	10.8	13.5
Half Angle at Pole (deg)	15	15
Number of Pole Pairs	2	2
Rotor Speed (rpm)	6000	6000
Field Energy (MJ)	0.397	0.486
Field Inductance per Turn ² (μH)	75.57	92.36
Weight of Stator Copper (lb)	239	210
Weight of Superconductor (lb)	372	421
Weight of Conductive Yoke (lb)	313	319

The rotors of these two machines differ only in active length; therefore, considerations affecting superconductor selection are the same for both machines. The winding in the study was modeled as an annular region with 30 degree poles and a current density of $15,000 \text{ A/cm}^2$. The winding to be used for the actual design consists of impregnated racetrack modules; this will result in a significantly different field distribution.

Figure 4 is a cross section of the rotor showing the winding configuration. The modules have a 3 inch bore and a cross section 2.85×2.94 inches. This configuration is not yet optimized, but it will serve for comparisons of superconductor characteristics.

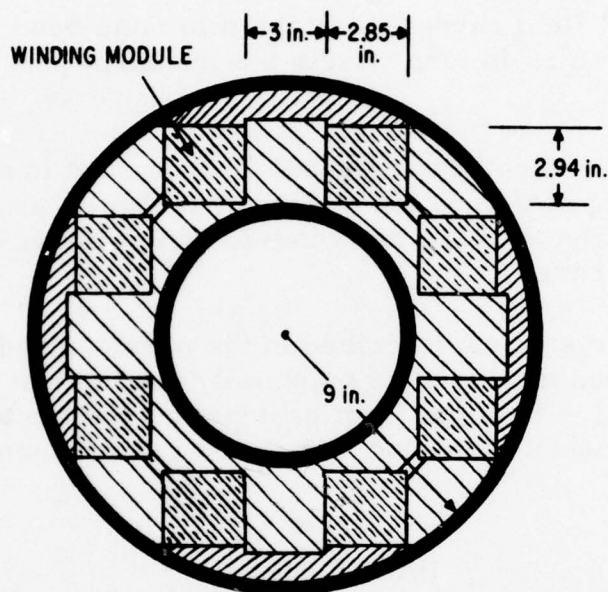


Figure 4. Winding Configuration

ANALYSIS

The field distribution generated by a four-pole winding constructed from racetrack-shaped modules requires either a finite element analysis or a Biot-Savart-law analysis applied to wire segments. The latter approach was selected, although it necessarily neglects the effects of the armature and the conductive environmental shield. These effects are of secondary importance in their contribution to the fields seen by the superconductor.

A General Electric computer program utilizing the Biot-Savart law was used, assuming each module consists of 40 wires. The semicircular end turns of the racetrack modules were approximated as one half of a ten-sided polygon. The computer program sums the field contributed by each wire segment, to yield the field magnitude and direction at any selected point.

FIELD DISTRIBUTION

In the Modules

A typical racetrack module is shown in Figure 5. Four sections and three planes are defined in this figure. The intersection of the planes with the sections defines twelve lines. The field distribution along these lines is plotted in Figures 6 to 9 for a module current density of $15,000 \text{ A/cm}^2$.

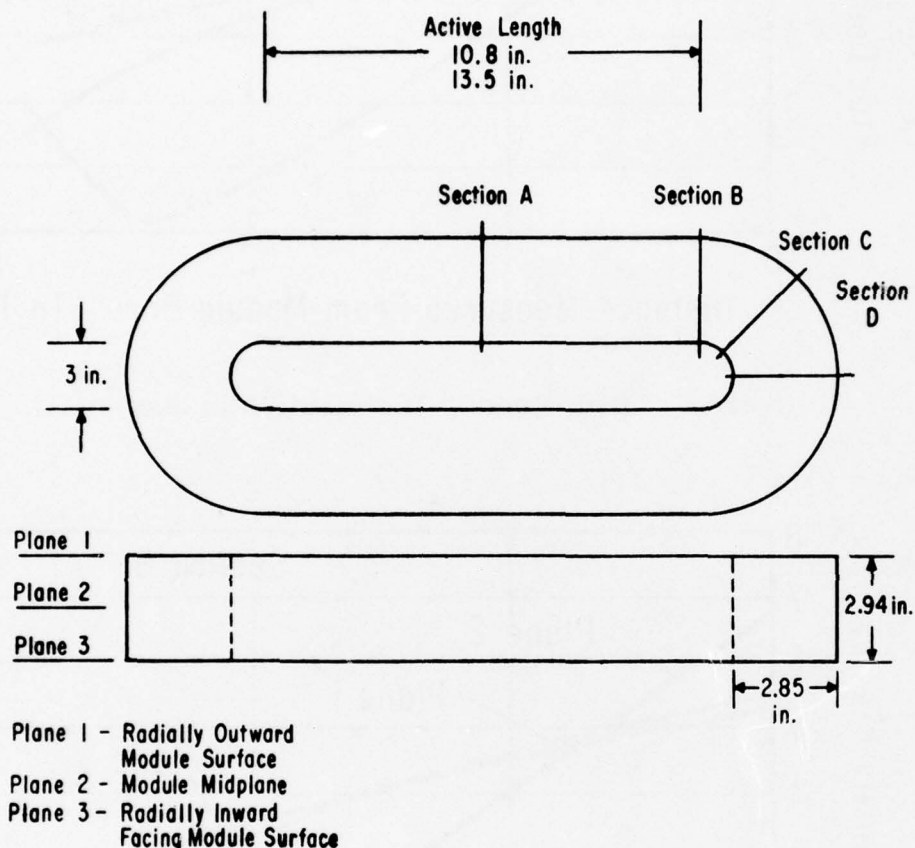


Figure 5. Module Configuration

The peak field of 6.8 T occurs in Section B near the inner surface of the module at the beginning of the end turn. It is important to note that the peak fields occur near the surface of the module. Further subdivision of the winding thus will not greatly increase conduction cooling of the peak-field region during field ramping.

The field magnitude is of interest in that it determines the conductor transition temperature for a given current density, but unless a cable or a round monolith is utilized, the losses associated with a one-second ramp will depend on both the magnitude and the field orientation.

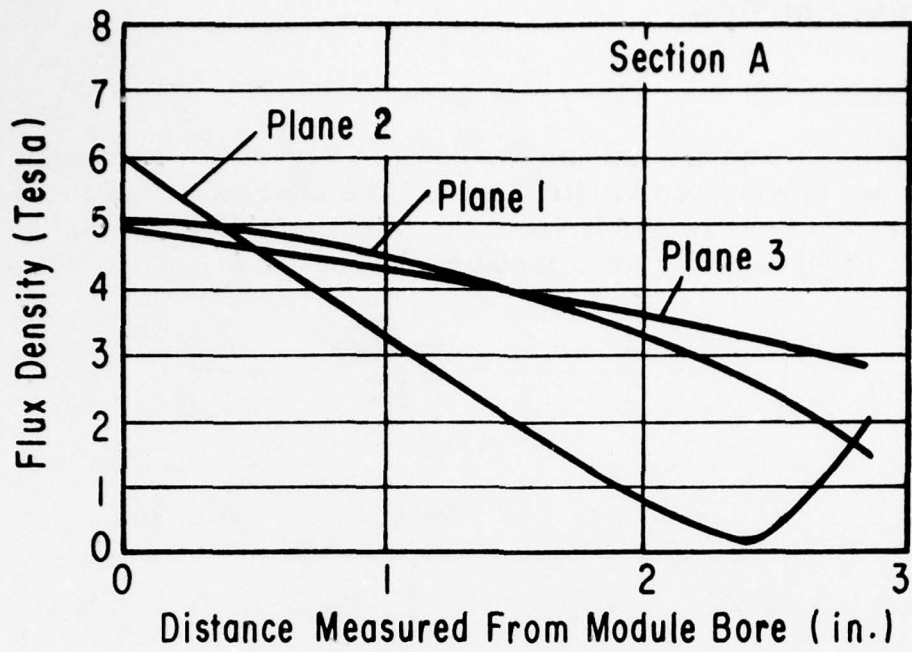


Figure 6. Flux Density Distribution in Section A

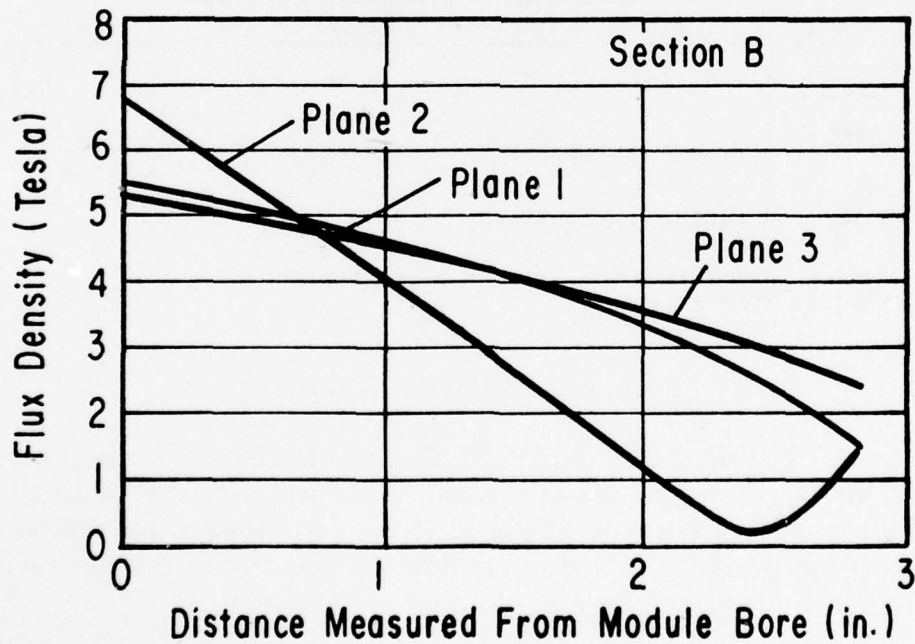


Figure 7. Flux Density Distribution in Section B

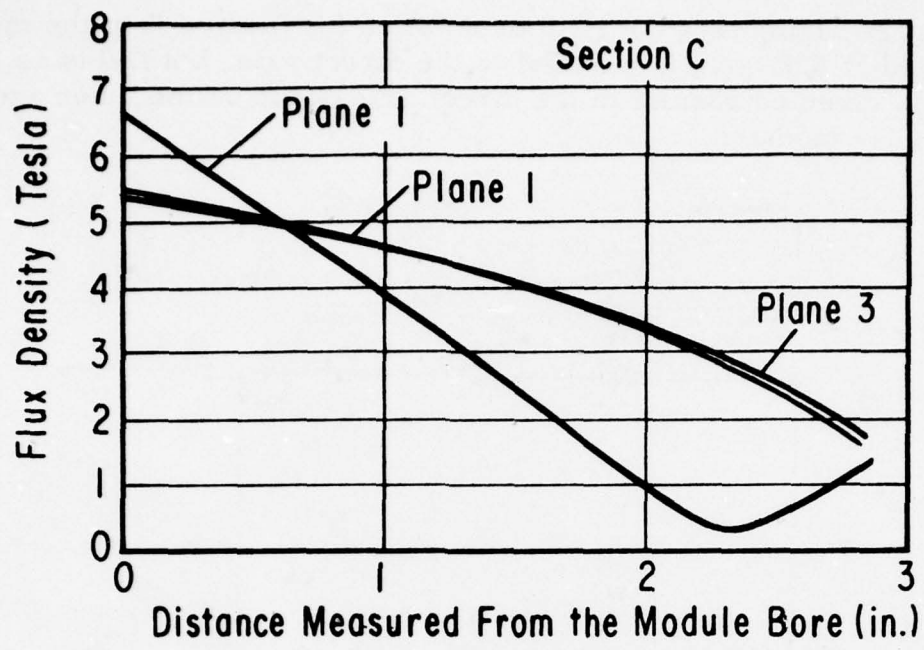


Figure 8. Flux Density Distribution in Section C

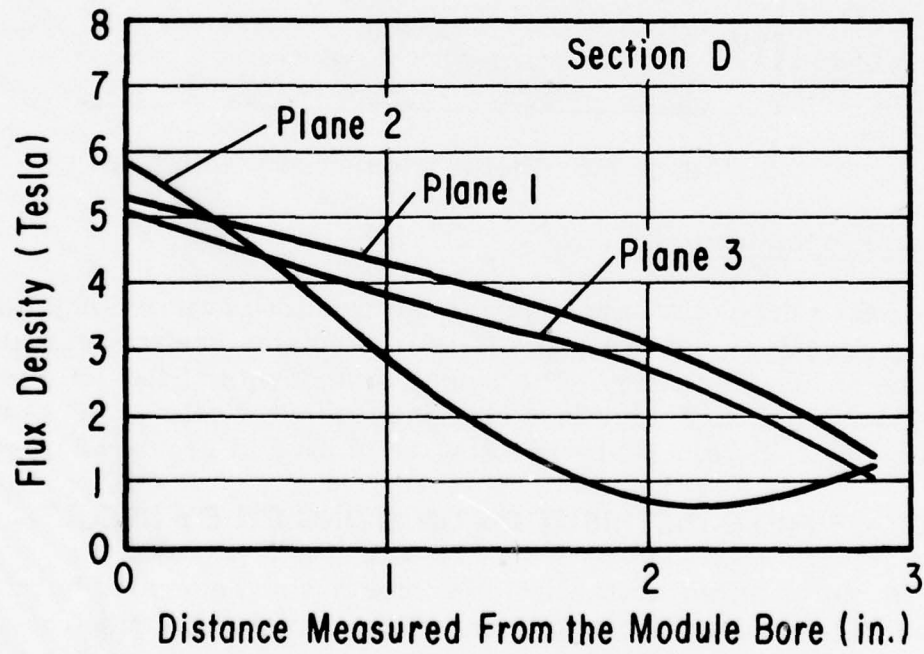


Figure 9. Flux Density Distribution in Section D

Figure 10 displays the field orientation for Section B of the module. The peak field of 6.8 tesla is parallel to the direct axis, but fields as large as 3.4 tesla directed normal to the direct axis occur on the inner and outer surfaces of the module.

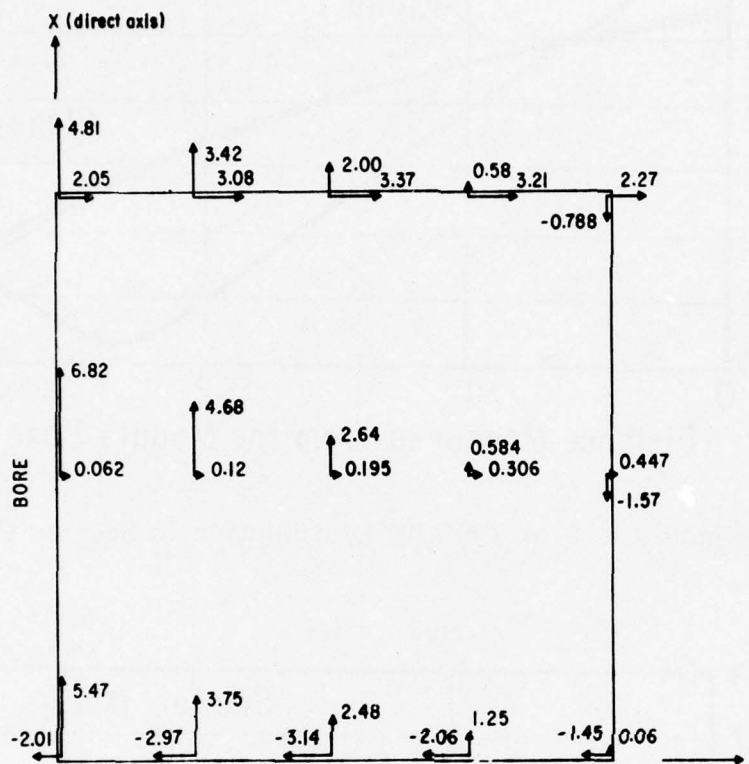


Figure 10. Field Orientation (Section B)

In the Armature

For the purpose of investigating the required active length of a rotor utilizing racetrack modules, the field in the armature was calculated at the midplane of the generator. The radial components of field at the inner ($r = 10.5$ inches) and outer ($r = 11.5$ inches) were calculated as a function of mechanical angle. These results are plotted in Figures 11 and 12.

EFFECT OF FIELD DISTRIBUTION ON SIZING STUDY RESULTS

With the detailed magnetic field information generated by the Biot-Savart law analysis, it is possible to quantify for the specific case the error inherent in the sizing study due to the assumption of annular-sector windings instead of rectangular-cross-section modules.

Since it is impractical to provide a racetrack configuration which accurately reproduces the fields assumed by the annular-sector model, it is convenient to devise a means to select the parameters of the annular-sector

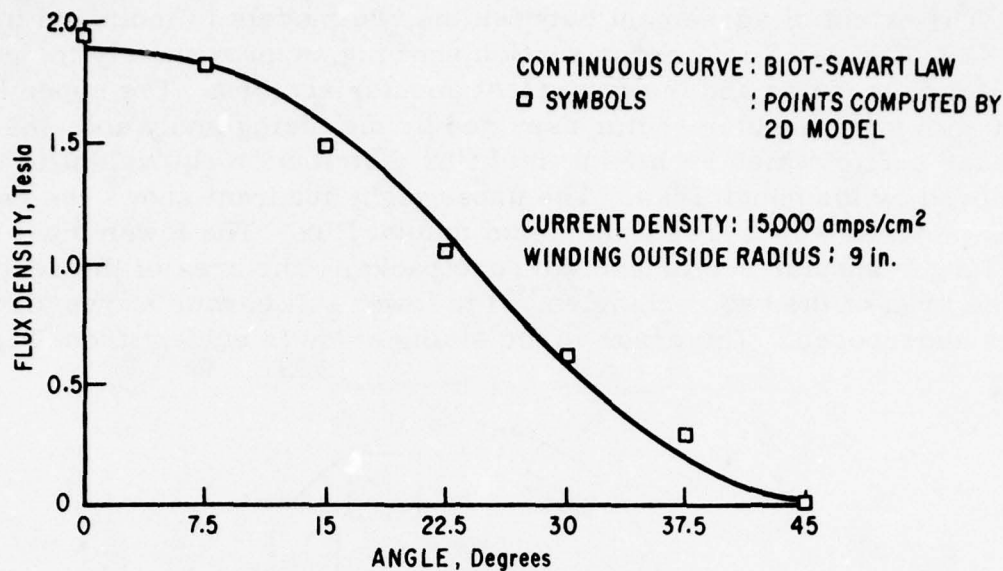


Figure 11. Comparison Between the Least-Squares-Fit, Two-Dimensional Model and Biot-Savart Law Radial Component of Magnetic Flux Density at $r = 10.5$ Inches

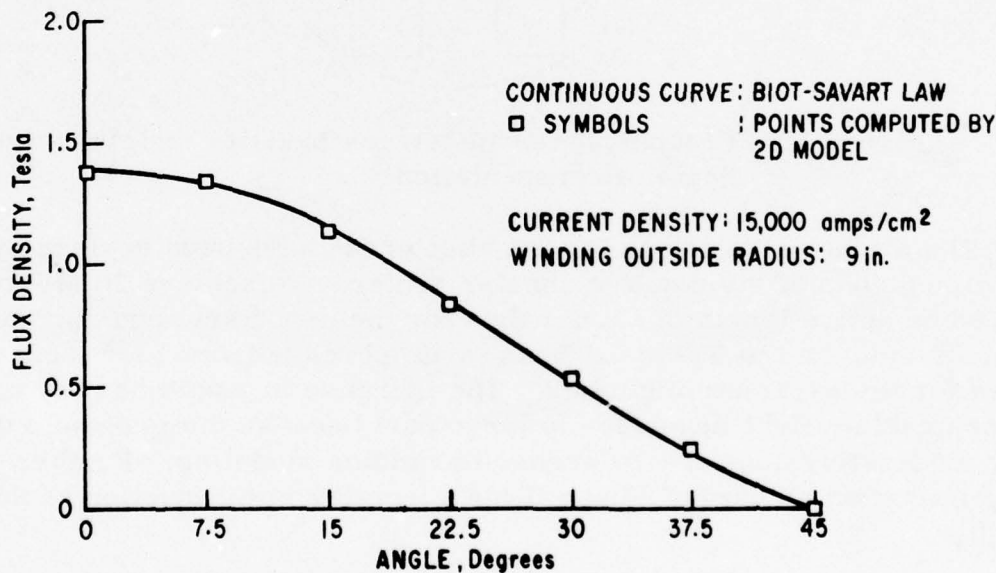


Figure 12. Comparison Between the Least-Squares-Fit, Two-Dimensional Model and Biot-Savart Radial Component of Magnetic Flux Density at $r = 11.5$ Inches

model to reflect the field distribution achieved by the racetrack design. It has proved possible to fix the annulus outside radius and current density to match the radius of the outermost point of the modules and module current density, and to select the annulus inside radius and pole-sector angle to provide a very reasonable least-squares fit of the annular-sector model to the racetrack module fields computed for the axial midplane by the Biot-Savart law.

The extent of agreement between the two models is indicated in Figures 11 and 12. Figure 13 is a cross section showing, approximately to scale, the racetrack modules and the equivalent annular sectors. The upper left quadrant shows the annular sector assumed by the sizing study and, inside it, the annular sector which creates a field flux distribution equivalent to that achieved by the racetracks. The upper right quadrant shows the two different shapes which create the same mutual flux. The lower right compares the larger annular sector and the racetracks. The area of the sector is equal to the area of the two rectangles. The lower left corner shows all three figures superposed. The error in the sizing study is evident from Figure 13.

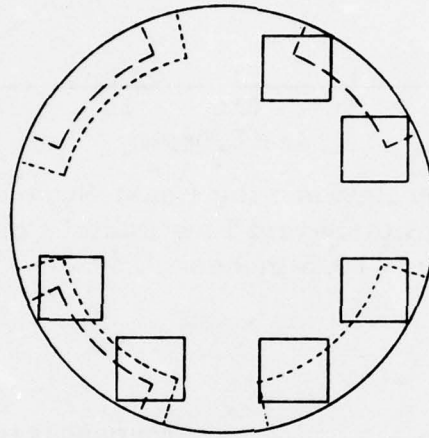


Figure 13. Comparison of Racetrack Modules and Annular-Sector Representation

The sizing calculations for the base cases have been revised by use of the dimensions of the smaller annular sector. To achieve 20 MW output required an active length of 17.6 inches for the concentric end-turn configuration, as indicated in Table 5. This is an increase from 13.5 inches as computed for the parametric studies. The increase in length has not caused an unacceptable weight increase, in large part because the four-pole design is only moderately sensitive to errors in winding modeling. Further parametric reoptimization as part of Phase II may permit some reduction of the active length.

Table 5

REVISED BASE DESIGN -- CONCENTRIC END TURN

Field Winding Current Density	15,000 A/cm ²
Stator Winding Current Density	600 A/cm ²
Inside Radius of Field Winding	7.28 Inches
Outside Radius of Field Winding	9.0 Inches
Inside Radius of Stator Winding	10.5 Inches
Outside Radius of Stator Winding	11.5 Inches
Conductive Yoke Radius	17.3 Inches
Active Length	17.6 Inches
Half Angle at Pole	23 Degrees
Number of Pole Pairs	2
Rotor Speed	6000 Rpm
Field Energy	0.311 MJ

Section IV

SUPPORT SYSTEM

The support system is analyzed as part of the process of selecting a superconductor, in order to verify that the base-design winding can be adequately supported.

DESIGN CONSIDERATIONS

The winding of a superconducting generator requires support against centrifugal and electromagnetic forces. This is the function of the rotor-winding support system, consisting of a torque tube, a support structure, and possibly a bore tube. In the configurations under investigation, the torque tube transmits torque, contains the winding, and serves as a vacuum barrier. The support structure serves to transmit winding forces to the torque tube.

Figure 14 presents the calculated loading for the base design field winding with a current density of $15,000 \text{ A/cm}^2$. Centrifugal acceleration loads the straight portions of the winding modules with a radial force of $15,500 \text{ lb/in.}$ of axial length. The electromagnetic force acts in the direction shown with a magnitude of $12,060 \text{ lb/in.}$ of axial length. This results in stresses at the surfaces of the module of 4800 psi and 6570 psi as shown in the figure. These low stresses indicate that high strength is not a requirement for the support structure. The tensile loading of the torque tube corresponding to these applied forces is $33,000 \text{ lb/in.}$ of axial length. If a thin torque tube is to be used to limit the size of the air gap, strength is an important consideration in the selection of the torque tube material.

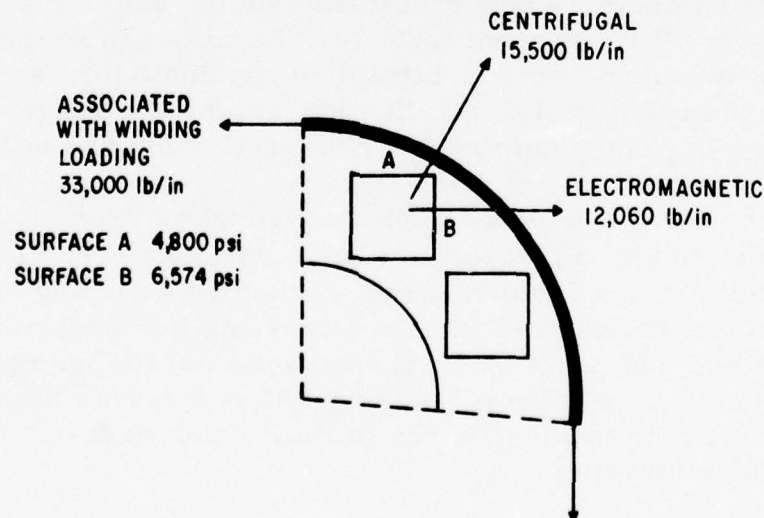


Figure 14. Winding Loading

Control of relative motion between the support structure and winding modules is an important consideration in selecting the support system materials and configuration. Heating at this interface caused by relative motion can cause premature quenching. This is particularly important in a design with the goal of achieving a one-second ramp to full speed and current.

SUPPORT SYSTEM CONFIGURATIONS

The growth of the torque-tube diameter with the application of load is a measure of the motion of the winding and support system. Since relative motion during sudden application of current and rotation is a primary consideration, the expansion of the torque tube during loading should be limited. This can be accomplished by constructing a thick torque tube of high modulus material or by prestressing the torque tube. Prestressing is more attractive in that increasing the air gap to accommodate a thick torque tube necessarily decreases the power density of the machine.

Prestressing the torque tube places the support structure in compression. The support structure has a large cross section in relation to the torque tube and therefore can be made stiff in comparison with the torque tube. The stiffness of the support structure may be further increased by adding a high-modulus bore tube.

When electromagnetic and centrifugal acceleration act on the winding, the inner portion of the structure and the bore tube are unloaded. Since the structure is relatively stiff, this results in only a small amount of radial motion. This radial motion increases the stress in the torque tube only slightly, since its stiffness is small compared with that of the support structure and bore tube.

Tables 6 and 7 compare potential materials for use in the torque tube and support structure. It is apparent from considerations of weight alone, that a glass-cloth/epoxy composite is an attractive candidate for use in the support structure. As indicated by Table 7, the low weight to strength ratio of the uniaxial-glass/epoxy composite makes it attractive for use in the torque tube.

Figure 15 presents one of the support system configurations under consideration, consisting of a composite support structure contained in a metallic torque tube banded with a filament wrap. Filament wrapping of the torque tube provides a convenient method of prestressing the torque tube with high-strength material. The axial thermal contraction of the impregnated filament relative to the metallic portion of the torque tube prevents the use of a continuous wrap. Narrow banding serves to limit axial stresses due to this relative thermal contraction.

This design includes a filament-wound bore tube to take the prestress compressive forces. A nonmetallic support structure and bore tube are desirable because they are loss-free during ramping. A thin metallic portion

Table 6
SUPPORT STRUCTURE MATERIALS

Materials	Density (lb/in ³)	Modulus (10 ⁶ psi)	$\Delta L/L$ (in/in.)	Resistivity ($\mu \Omega m$)
Aluminum	0.1	10	0.004	0.0138
Titanium	0.163	17	0.0015	1.4
Steel	0.28	30	0.003	0.5
Glass				
Composite	0.06	4	0.0013	∞

Table 7
TORQUE TUBE MATERIALS

Material	Yield (10 ³ psi)	Density (lb/in ³)	ρ/σ_y (10 ⁶ lbm/in ³ /psi)	Modulus (10 ⁶ psi)	$\Delta L/L$ (in./in.)	Resistivity ($\mu \Omega m$)	$\omega^2 R^2 \rho$ (10 ³ psi)
Inconel X-718	170	0.298	1.75	31	0.0024	0.99	26
Glass Filament	240	0.060	0.25	9	0.0013	∞	5.2
Titanium	191	0.163	0.85	17	0.0015	1.4	14.2

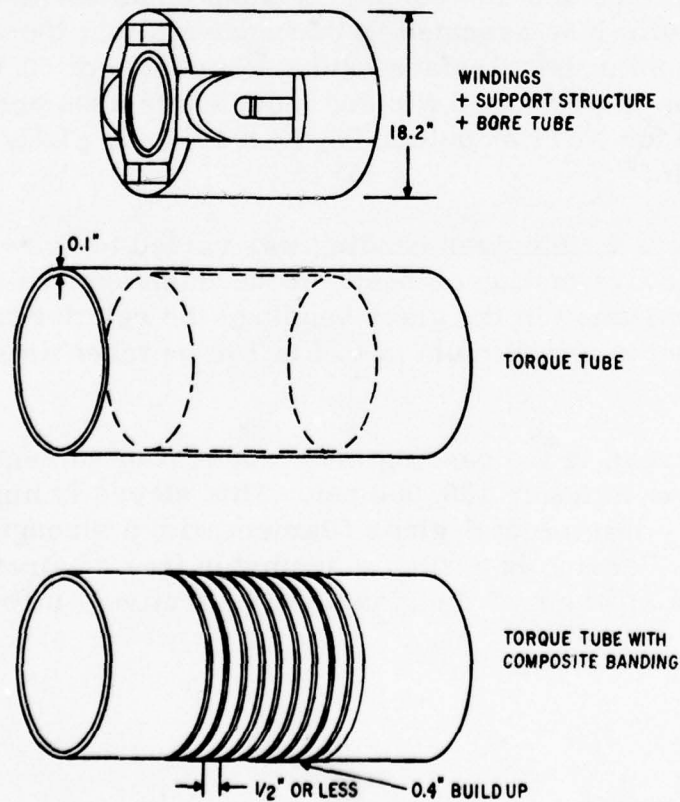


Figure 15. Support System Design Concept

of the torque tube is required to provide a vacuum barrier, but the major part of the torque tube, consisting of filament banding, is also loss-free.

Other support system configurations are under consideration:

- An all-metallic torque tube, composite support structure, and metallic bore tube.
- A configuration similar to that presented in Figure 15, with the location of the metal and filament banding in the torque tube reversed.

ANALYSIS

The support system depicted in Figure 15 was selected for initial investigation. Figure 16 presents the finite element representation of the winding and support system, which was investigated with a two-dimensional finite-element computer program. This analysis has been used in an iterative design process to arrive at the dimensions shown. The criteria for selection were the peak stresses in the structure and the relative motion at the winding/support-structure interface.

Two important inputs to the analysis are the assumed mechanical characteristics of the interface and the winding module. Experience has shown that introducing a low-modulus material between the module and the support structure prevents slippage at the module interface. Relative motion between the support structure and the winding is taken up as shear strain in the low-modulus material. It is assumed in this analysis that there is 0.01 inch of isotropic material at the interface having a modulus of 60,000 psi. The characteristics of the impregnated winding module are assumed to be similar to those measured for NbTi modules: $E = 3 \times 10^6$ psi; $\Delta L/L = 3.4 \times 10^{-3}$ in./in.; $\rho_{\text{avg}} = 0.27$ lb/in.³

The prestress in the glass banding was varied to determine the effect of prestress on relative motion or shear at the interface. If a prestress of 120,000 psi is assumed in the glass banding, the relative motion during loading is limited to a maximum of 0.7 mil to be taken as shear in the interface material.

The peak stress in the banding after application of centrifugal and electromagnetic loads is under 130,000 psi. This stress is high but realistic, when considering the use of S-glass filament with a strength well in excess of 200,000 psi. Banding is a simple geometry free of stress concentrations which allows the strength of the glass to be effectively utilized.

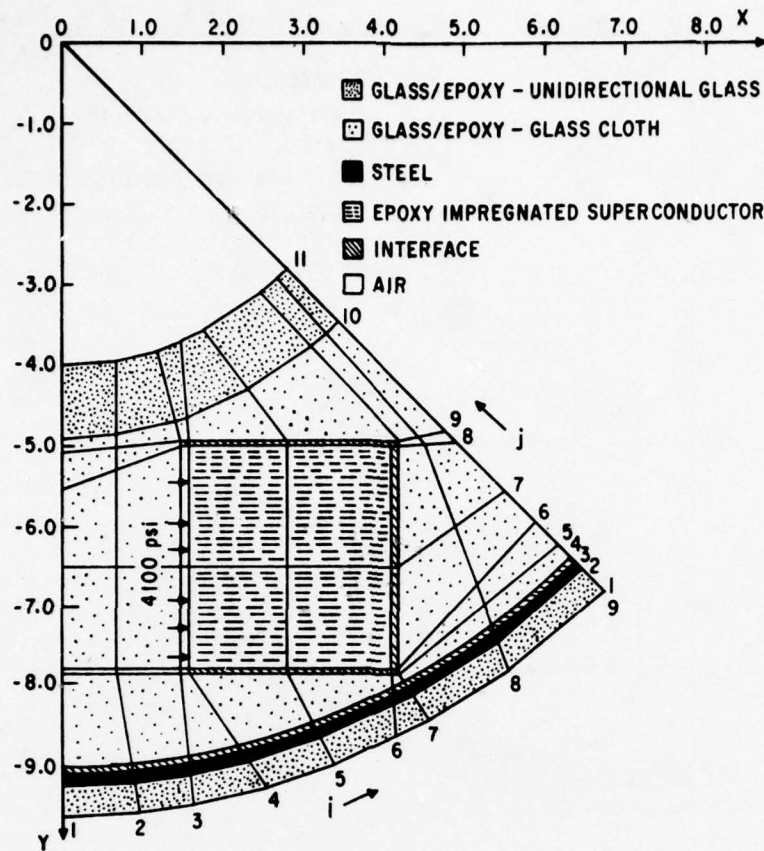


Figure 16. Winding and Support System Finite-Element Representation (Composite Torque Tube)

The stresses in the remaining parts of the support system are relatively low. The peak stress in the support structure is 11,000 psi, while the peak stress in the winding modules is 8530 psi.

The rotor grows only 0.005 inch radially during application of load, indicating that prestressing is an effective method for limiting the rotor dimensional changes during loading. If prestressing had not been used, the rotor would have grown 0.08 inch radially with application of load. Even if a 0.5-inch-thick steel torque tube were assumed in a nonprestressed configuration, the rotor would grow 0.025 inch radially.

A second support system was also investigated. Figure 17 is the finite-element representation used to model this system. The torque tube is entirely metallic (Inconel X718™), the support structure is of similar construction and material to that assumed in the previous analysis, and the bore tube is titanium. The bore-tube thickness has been reduced to take advantage of the stiffness of titanium.

™Trademark of the Huntington Alloys Inc.

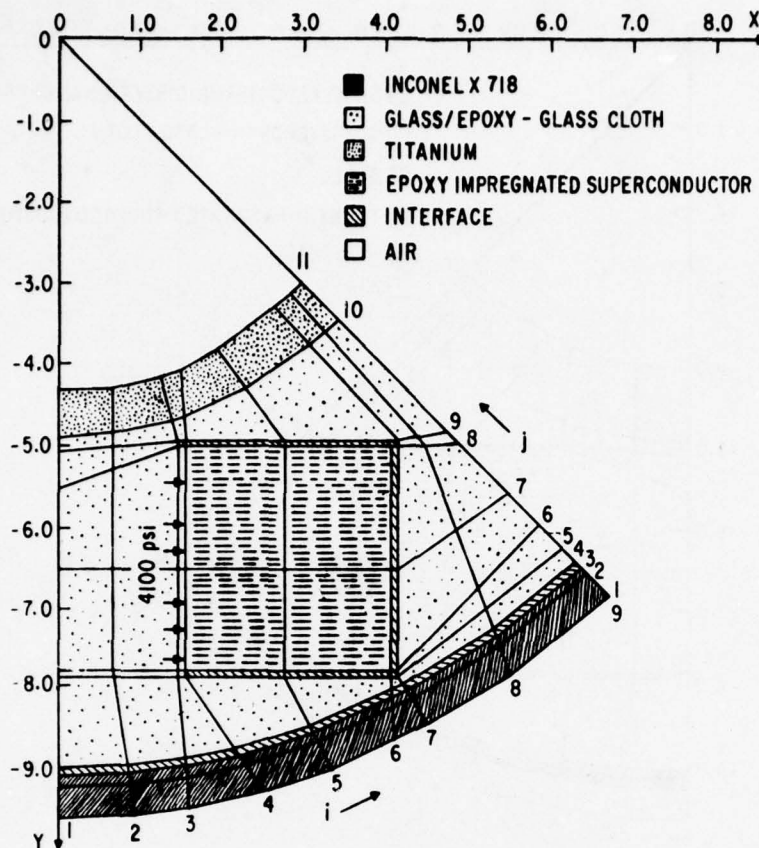


Figure 17. Winding and Support System Finite Element Representation (Metallic Torque Tube)

The torque tube is prestressed in this configuration by cooling the support structure with liquid nitrogen before assembly in the torque tube. The thermal contraction of the Inconel prestresses the torque tube.

The finite-element analysis was utilized to investigate the stress in the support system and relative motion between the support structure and the modules with the application of loading. The torque tube stress was found to be approximately 90,000 psi.

The torque tube radius was found to increase approximately 0.006 inch with the application of loading, and the relative motion between the support structure and the modules was determined to be less than 0.002 inch. This is a larger relative motion than was calculated for the glass-banded system, but experience with NbTi winding modules indicates this shear can be taken in the interface material without frictional heating. The larger value of relative motion with loading for this system is due in part to the lower prestress achievable with a metallic torque tube.

Ramping-loss estimates in the bore tube and torque tube indicate the loss will be less than 350 joules, which is sufficient to boil only one-seventh of a

liter of liquid helium. The computed adiabatic temperature rise of these structures is well above the critical temperature of the superconductor. The bore tube and torque tube must be well insulated from the modules.

SUMMARY

The base-design winding configuration can be adequately supported. A composite support structure appears attractive from weight and ramping-loss considerations; several torque tube configurations are being considered. Pre-stressing of the torque tube will be necessary for all configurations, to limit rotor growth and resulting relative motion at the module interface during loading.

32

Section V

ELECTROMAGNETIC SHIELD

FUNCTION AND REQUIREMENTS

It has long been recognized that the proper functioning of the rotor shield system is essential to the successful operation of a superconducting alternator. The several functions of the shield system place conflicting pressures on selection of shield parameters, and the proper design of rotor shielding remains a subject for study.

Most studies have confirmed the benefit of using separate components to perform the thermal and electromagnetic shielding functions. The electromagnetic shield experiences heavy crushing and torsional loads and carries large surface currents. Therefore, it is often placed at or above ambient temperature to make possible both adequate support and economical cooling. With separate shields, the electromagnetic performance of the thermal radiation shield is of importance principally in determination of the electromechanical loads on the thermal shield.

Assuming that thermal radiation shielding requirements are satisfied by a separate member, the remaining requirements of the electromagnetic shield may be cataloged as follows.

Adequate Magnetic Field Attenuation vs Frequency

An isolated machine feeding a rectifier is fairly easy to specify in this respect. The frequencies and amplitudes of the principal components of the nonsynchronous magnetic field may be determined and the required field attenuation specified. The system design will be sufficiently symmetric so that phase unbalance can be kept small. In synchronous operation, the desire to damp speed variations limits the extent to which a single high-conductivity shield may be relied upon for shielding of steady-state asynchronous fields. No such limitation arises in the present case. Adequate shielding can be achieved by selection of a material with an electrical conductivity such that a mechanically adequate shield has a sufficient magnetic field attenuation. In practice, this suggests relatively high-conductivity materials; aluminum alloys are especially attractive.

Adequate Torsional Strength

The electromechanical shear load on the shield surface following a short circuit may be many times rated torque. The shield must survive application of such a load. For the case at hand the shield is at a large radius, and the required thickness will not be excessive if a good structural material is chosen.

Adequate Strength for Crushing Load

The crushing loads which arise following a sudden short circuit on the armature have been a major concern in the design of superconducting alternators. Adequate strength to survive these loads is often the factor which governs selection of shield thickness and material. In the present case of a generator feeding an isolated load, it is anticipated that occurrence of a short circuit will require system shutdown. Under these circumstances, it may be acceptable to permit the electromagnetic shield to contact the cold rotor body. Torsional strength then becomes the limiting requirement; the required shield thickness is substantially reduced, and significant improvements in output per unit weight may be achieved.

Acceptable Natural Frequencies

The natural frequencies for ring-mode vibration of an electromagnetic shield have been shown to depend on speed of rotation and on the magnetic field magnitude in addition to the conventional mass and elastic stiffness parameters. Computation of the magnetic field effects on natural frequency is in a fairly primitive state of development, and as a result, natural frequencies in operation are not precisely known. Different space and time harmonics of magnetic field can combine to create driving forces for any of several modes at any of several frequencies.⁵ Considerable care may be required to insure that the computed ring-mode frequencies are sufficiently different from the frequencies of all available driving forces to allow for possible errors in the computation.

MATERIAL AND THICKNESS SELECTION

Preliminary calculations have suggested that a mechanically adequate shield of aluminum alloy would provide sufficient shielding. To make the shield as thin as possible, a high-strength alloy, 7178T6, is tentatively selected. If the philosophy is adopted that the shield may be supported by the rotor during short circuits, the capability to survive short-circuit torque is the limiting requirement. The revised baseline generator design (one-inch-thick armature, 17.6-inch straight length) exhibits a very low subtransient reactance, resulting in very high short-circuit torques. For a three-phase short circuit from open circuit, assuming constant voltage behind subtransient reactance, the peak torque is

$$T_{\max} = 1/X_d'' \quad (1)$$

where all parameters are expressed in a per-unit system on the machine rating. For $X_d'' = 0.0482$, $T_{\max} = 21$.

The corresponding design torque is

$$T_{\max} = 21 \frac{20 \text{ MW}}{2\pi(100/\text{sec})} = 6.68 \times 10^5 \text{ n-m} = 5.92 \times 10^6 \text{ in-lb} \quad (2)$$

Using the thin-wall theory and the maximum shear stress criterion, the thickness required to withstand both the hoop stress due to centrifugal load and the shear stress due to torque is

$$t = \frac{T_{\max}}{\pi} \frac{1}{R^2} \left(\frac{1}{\sigma_y^2 - (\rho R^2 \omega^2)^2} \right)^{1/2} \quad (3)$$

where: R = shield radius
 σ_y = tensile yield stress of material
 $\rho R^2 \omega^2$ = centrifugal pressure

For $R = 9.9$ inches, $\sigma_y = 78,000$ psi, $\rho = 0.1$ lb/in³, and $\omega = 628$ /sec,

$$t = 0.25 \text{ inch} \quad (4)$$

This thickness is compatible with the allowance made in arriving at the baseline design. If a shield of this material and thickness can be shown to be acceptable in other respects, the overall performance goals of the design should be achieved.

SHIELDING REQUIREMENTS

When an ac generator feeds a rectifier load, the dominant source of non-synchronous magnetic field is the nonsinusoidal nature of the armature currents. This effect exists even under conditions of perfect phase balance. In a small, isolated system, such as this one, phase unbalance can be controlled by careful design. Limitation of the ac field seen by the rotor, due to current waveform, is accordingly the condition which determines the steady-state shielding requirement in a superconducting generator designed for rectified load. An understanding of operation into rectified load is required, to permit adequate shield design.

A recent paper by Stuart and Tripp⁶ outlines a procedure to evaluate all the parameters necessary to obtain a detailed closed-form description of the behavior of an ac generator with rectified load. Using the procedure indicated, shield-winding currents can be obtained for the case of a perfectly conducting shield, from which can be derived an estimate of ac field with a shield of finite conductivity.

The amplitudes, i_{d1} and i_{q1} , of the fundamental components of shield-winding currents on the two rotor axes are readily obtained. These currents can be imagined to be the result of currents at the same frequency in the d and q windings of the armature:

$$I_d = \frac{2}{3} \frac{L_d}{M_d} i_{d1} \cos(2\pi f_o t) \quad (5)$$

$$I_q = \frac{2}{3} \frac{L_d}{M_d} i_{q1} \sin(2\pi f_o t) \quad (6)$$

The corresponding flux density distribution in the absence of shielding currents can then be determined from two-dimensional field equations. If the influence of the environmental screen is ignored, magnitude of the spatial fundamental is independent of angle, and for a four-pole machine, linear with radius r ,

$$|B| = K \sqrt{I_d^2 + I_q^2} r \quad (7)$$

For the baseline configuration, at $r = 9$ inches, this works out to

$$|B| = 33 \text{ gauss} \quad (8)$$

This field fluctuation occurs at 1200 Hz. For the proposed shield, $\rho = 5.5 \times 10^{-8} \Omega\text{-m}$ and the thin-shield time constant is

$$\tau = \frac{\mu \sigma R \Delta}{2} = 0.0182 \text{ sec} \quad (9)$$

where Δ = shield thickness.

Assuming the field winding is open, and neglecting the effect of closed circuits in other conductive members, the field is reduced by a factor of $1/(1 + \omega \tau) = 1/139$ to 0.24 gauss. Conservative computations indicate that shielding to a level of 1 gauss is adequate, even at twice the frequency of interest,⁷ so this level of shielding is quite acceptable.

The calculation presented above makes several potentially significant simplifications. The field winding will behave more nearly as if it were short-circuited than as if it were open. The field due to induced field-winding currents will be superposed on the field due to armature and shield currents, making the resultant field larger in some places and smaller in others. Space harmonics should be added, of course. Other conductive members will carry currents, in this case probably improving overall shielding effectiveness. Finally, the shield is nearly two skin depths thick at the frequency of interest; this should result in some shielding improvement at 1200 Hz and much more at time harmonic frequencies.

CONSIDERATIONS OF CRUSHING LOAD

The fundamental component of crushing load, following a sudden three-phase short circuit from open circuit, is of the form

$$\sigma_m = P_o (1 + \cos(4\theta)) \quad (10)$$

The peak bending moment corresponding to this pressure is

$$M = 0.13368 P_0 R^2 l \quad (11)$$

where R is the undeformed radius and l is the axial length. From curved-beam theory, the peak tensile stress due to a static load of the form of Equation 10 is

$$\sigma = \frac{6M}{t^2 l} \quad (12)$$

For $P_0 = 480$ psi, $R = 9.9$ in., and $t = 0.25$,

$$\sigma = 600,000 \text{ psi} \quad (13)$$

This is far beyond the bounds of practicality. If subtransient reactance can be increased by a factor of 4 or so, it may be possible to thicken the shield enough to withstand the crushing load. If this alternative is undesirable it may be permissible during such severe transients to permit the shield to derive support from the torque tube, with the radiation shield trapped between. The peak deflection due to a load of the form of Equation 10 is

$$\delta = \frac{12}{225} \left(\frac{R}{t} \right)^3 \left(\frac{P_{\max}}{E} \right) R \quad (14)$$

If E is 10^7 psi, Equation 14 indicates that δ would be 1.51 inches if the shield were capable of 600,000 psi. To keep the peak stress at a reasonable value (say 50,000 psi), the deflection must be limited to

$$\delta_1 = \frac{50,000}{600,000} 1.51 = 0.125 \text{ inch} \quad (15)$$

This value of δ_1 should be sufficiently large to allow for easy assembly and for any normal variations in radial clearance as temperature change.

SHIELD VIBRATION

Ring-mode vibrations of thin cylindrical shields have proved to be a problem in superconducting generators. Excitation forces for such motions can be generated by action of the magnetic field on the current induced in the shield by asynchronous armature fields. The natural frequency for ring-mode motions can be influenced by rotational speed and by the magnetic field level, so the possibility exists to tune or detune the system by variation of the operating point. Apart from the stress and fatigue questions associated with operation near a critical speed, the resulting shield motion creates a time-varying magnetic field which can be a significant source of field-winding heating. Excitations may exist for any of several modes at any of several

frequencies. For a four-pole generator feeding a rectifier, the largest excitation will be for the mode having eight nodes (a $\cos(4\theta)$ angular dependence) and will occur at 6 times the electrical frequency (1200 Hz in the present case).

Using the methods described by Shevchuk,⁸ one can determine that the eight-node natural frequency at standstill is 393 Hz, assuming simple end supports and a length of 34 inches. When the effects of rotation are taken into account, the natural frequency splits into two values, one for forward-running and one for backward-running waves. These values are 575 and 481 Hz respectively.

The magnetic stiffening computations proposed by Shevchuk depend critically on identification of an "effective spacing," which is the radial distance from the shield to some radius within the field winding at which the field winding can be presumed to be concentrated. No ready means is available to make this identification. As the effective spacing is varied from 3 to 1 inches, bracketing the range of possible values, the natural frequencies sweep through the range between 778 and 1300 Hz. Clearly, the possibility of shield vibrations will require careful attention during the design phase.

SUMMARY

The basic magnetic field attenuation and torque transmission capabilities can be achieved with a 1/4-inch-thick tube of ambient-temperature structural aluminum. Such a shield can withstand the crushing loads of a suddenly applied short circuit if it is allowed to bottom on the rotor body. Modification of the machine to achieve a nonbottoming shield would require a thicker (higher-reactance) armature and probably a thicker shield as well. An extreme change in either dimension will carry a weight penalty.

Shield vibration is a potentially difficult problem. An analytical technique is required to predict magnetic stiffening effects with reasonable precision. The alternative is a design modification to raise all possible natural frequencies above the available excitation frequencies. The thickness required to do this with mechanical stiffness would probably require an increased gap between field and armature, with an associated severe weight penalty. Intentionally augmented magnetic stiffening should not require so much space, and deserves more attention for this application.

The selection of a shield which is suitable in all respects is not an easy task, and should properly be performed only in the context of a complete machine design. But the preliminary calculations presented here are sufficient to show that the baseline designs chosen for superconductor selection calculations are attainable.

Section VI

SUPERCONDUCTOR SURVEY

INTRODUCTION

The superconductor survey is intended to be an investigation of the characteristics of superconductors currently manufactured or under advanced development. Domestic and foreign manufacturers were contacted and asked to provide information on existing or proposed superconductors meeting certain specifications. These specifications are included in this report as Appendix A. These rather broad requirements were based on a preliminary investigation of the 20 MW generator and its advanced superconducting rotor.

RESULTS

Table 8 is a listing of the manufacturers who were asked to complete the survey; the responding manufacturers are indicated. The completed forms are included in Appendix B. In addition to this list, the Aluminum Company of America was contacted concerning aluminum stabilized superconductors.

Table 8
SUPERCONDUCTOR SURVEY

Manufacturer	Responded
<u>USA</u>	
Intermagnetics General Corporation (IGC)	✓
Airco, Inc.	✓
Magnetic Corporation of America Supercon, Inc.	✓
<u>England</u>	
Imperial Metal Industries Limited U.K. Atomic Energy Research Establishment	
<u>Germany</u>	
Vacuumschmelze	
<u>Japan</u>	
Toshiba Shibaura Electric Co., Ltd.	✓
Hitachi, Ltd.	✓
Sumitomo Metal and Mining Co., Ltd.	

The survey was intended to include superconductors other than Nb_3Sn , but Nb_3Sn conductors were proposed by the majority of the manufacturers because of the ramping requirements.

The majority of responses are from IGC and Airco. Each responded with both cabled and monolithic multifilamentary superconductors in a variety of sizes. Supercon, Inc., responded with two conductors--cabled Nb₃Sn and NbTi. The Magnetic Corporation of America did not formally respond; they indicated that this was because Nb₃Sn is the proper conductor for the application, and they are in the early development stage with this conductor. The United Kingdom Atomic Energy Research Establishment (Harwell) and Imperial Metal Industries Ltd., did not respond. Hitachi responded with two large cabled conductors--Nb₃Sn and NbTiZr. Toshiba responded with a cabled Nb₃Sn conductor. Vacuumschmelze did not wish to formally respond until more detailed list of requirements is furnished. Sumitomo also did not complete the survey form; they felt that their conductor did not address our specific requirements.

The IGC conductors are in various stages of development. Conductor E has been developed by IGC and can be delivered within four to six months of an order. The other conductors are being developed as part of an Air Force funded program. Delivery of these conductors is expected to be possible within six months of an order placed in January of 1978.

Short lengths of the Airco conductors have been manufactured and are being tested. The Supercon Nb₃Sn conductor is a proposed conductor and has not been manufactured. The Hitachi conductor is also new and would require additional development. Short lengths of the Toshiba conductor are currently available.

SURVEY RESULTS AS APPLIED TO THE BASE DESIGN

The winding design discussed in Section V results in the following operating condition for the superconductor:

$$B_{\text{peak}} = 6.8 \text{ tesla} \tag{16}$$

$$J_{\text{conductor}} = 20,000 \text{ A/cm}^2$$

The conductor current density results from an assumed module current density of 15,000 A/cm² and a packing factor of 75 percent. "Packing factor" is defined in this instance as the percentage of the module cross section which consists of superconductor composite, not including the superconductor insulation. This is a reasonable packing factor for a rectangular monolith, but it may be difficult to obtain with a round or cabled conductor.

The proposed NbTi and NbTiZr conductors do not have sufficient temperature margin to withstand a one-second ramp to this operating point. Nb₃Sn is therefore preferred, and the proposed Nb₃Sn conductors are compared for the required operating condition in Table 9. The critical temperature corresponding to this operating point may be estimated from typical Nb₃Sn characteristics.⁹ The estimated critical current for each Nb₃Sn conductor is listed in Table 9.

Table 9
BASE DESIGN SUPERCONDUCTOR COMPARISON

<u>Conductor</u>	<u>Loss (mJ/cm³)</u>	<u>T_c (°K)</u>	<u>I (amps)</u>	<u>Cu (%)</u>	<u>Cost (K\$)**</u>	<u>Bend Rad (cm)</u>
<u>IGC</u>						
A Cable	21 - 74	8	235.4	43	97 - 137	1.63
A' Cable	81 - 296	8	942	43	97 - 137	3.3
B Monolith (aspected)	21	5	200.9	68.5	78 - 113	1.27
B' Monolith (aspected)	82	5	803.6	68.5	78 - 170	2.54
C Monolith (aspected)	58	9	305	40.5	97 - 137	3.81
D Monolith (round)	17	9	63.3	45.5	97 - 121	2.16
E Cable	17	10	58.4	10	70 - 94	2.03
<u>Airco</u>						
A Monolith (aspected)	*	9	91.2	25	49	2.5
B Monolith (aspected)	*	9	210.7	34	59	3.8
C Monolith (aspected)	*	9	168.4	50	40	3.8
D cable	*	9	14.13/strand	30.6	78	2.5 - 4
<u>Supercon</u>						
Cable	46	9	1,161	50	102	7.6
<u>Hitachi</u>						
Braid	2.8	<4	1,520	12	73***	3.8
<u>Toshiba</u>						
Cable	*	6	122	64	100	7.2

Loss - Estimated for one-second ramp to 6.8 tesla from supplied values.

T_c - Estimated for 20,000 A/cm² at 6.8 tesla.

I - Current at 20,000 A/cm².

* - Airco and Toshiba did not estimate losses.

** - 0.69 ft³ estimated requirement (revised base design).

*** - Plus development costs.

The losses for a one-second ramp to 6.8 tesla are estimated by assuming the loss has the following form:

$$\text{Loss} = C_1 (B) + C_2 (B)^2 \quad (17)$$

The survey results for a one-second ramp to 4 and 8 tesla were used to calculate the constants C_1 and C_2 for each conductor. Equation 17 was then used to calculate the losses for each conductor for a ramp to 6.8 tesla in one second.

The bend radius required for the base design is 1.5 inches, or 3.81 cm. Supercon's cable and Toshiba's cable are the only proposed conductors which will not meet this requirement.

CABLED SUPERCONDUCTORS

Cables proposed by several manufacturers are included in Table 9. In addition to the listed cables, several of the monolithic conductors can be wound in a cabled configuration. In particular, IGC conductor D is a small cross-section monolith which IGC plans to test in a cabled configuration consisting of six strands wrapped around a molybdenum core.

Cables such as these have the obvious advantages of low ramping losses and small bending radius in sizes compatible with high currents. The disadvantages of cabled conductors have to do with the insulation and epoxy impregnation system. The impregnation system relies on the conductor being insulated with a polyvinyl formal coating. Polyvinyl formal bonds well to copper, and epoxy wets and bonds well to the polyvinyl formal.

The impregnation system in current use is not directly applicable to Nb_3Sn cables. Polyvinyl formal cannot be applied before cabling, because the reaction temperatures are too high for this insulation. The wire cannot be reacted before cabling because the bend radius for cabling is too small for the reacted conductor. Insulating cable with polyvinyl formal will result in a structure of uncertain mechanical integrity, and the insulation may inhibit strand slippage in the cable during bending. Cables rely on strand slippage to allow small-radius bends without subjecting the outer wire to severe strains.

Modification of the impregnation system will be necessary if a cabled conductor is to be used. One alternate system consists of wrapping the un-insulated cable with glass cloth. Experience indicates that epoxy does not wet or bond well to copper unless the copper is subjected to extensive surface preparation such as etching, priming, or plating. This system may prove successful with further development.

An alternate system consists of wrapping each strand with quartz cloth prior to cabling and reaction. The epoxy may flow into the cable through the wrap. This scheme may allow complete impregnation of the cable, but it does

not guarantee good bonding between the conductor and the epoxy. If complete impregnation of the cable is achieved, epoxy bonding may or may not be required for good coil performance. As with the previous system, development is required.

It can be concluded that cables are a promising conductor type for this application, but their selection is contingent on successful development of the impregnation process.

Section VII

FIELD RAMPING

INTRODUCTION

The transient performance of an impregnated superconducting module is a function of the heat capacity and thermal conductance of the composite, the field distribution and orientation, and the selected superconductor. For a round, cabled, or square conductor the transient performance is insensitive to the orientation of the field. To obtain an estimate of the base-design winding performance a transient heat-transfer computer program was utilized to determine the temperature distribution in a module following a one-second ramp to operating current, assuming the conductor losses to be insensitive to field orientation.

As shown in Figure 10, the field in a module is not unidirectional. The effects of field orientation were then investigated to determine the applicability of the transient analysis to a highly aspected conductor.

The voltage requirements placed on the winding insulation by the one-second-ramping goal can be severe. Ramping voltages were calculated for the revised base design.

COIL COMPOSITE PROPERTIES

Values of specific heat and thermal conductivity are required as inputs to the transient thermal analysis of the modules. Prior to the selection of a specific conductor these properties are by necessity estimates.

For the purpose of estimating the composite specific heat, the following module composition was assumed:

Copper and Bronze	56.8%
Glass and Epoxy	25 %
Tantalum	9 %
Nb ₃ Sn	9.2%

Reference 10 presents the specific heat of Nb₃Sn as a function of temperature, and Reference 11 was used to estimate the specific heat of the remaining materials. Equation 18 was used in the transient thermal analysis to approximate the specific heat of the composite:

$$c_p = 9.04 \times 10^{-6} T^{2.32} \text{ J/gK} \quad (18)$$

The thermal conductivity of the composite is dominated by that of the epoxy and glass (polyvinyl formal is assumed to have thermal properties identical to epoxy). Glass cloth is included between layers in the module to

provide layer-to-layer insulation. Because of the interlayer insulation, even if a rectangular or round conductor is used, the thermal conductivity is greater in the direction parallel to the direct axis. Figure 18 is a schematic diagram indicating the conductor spacing.

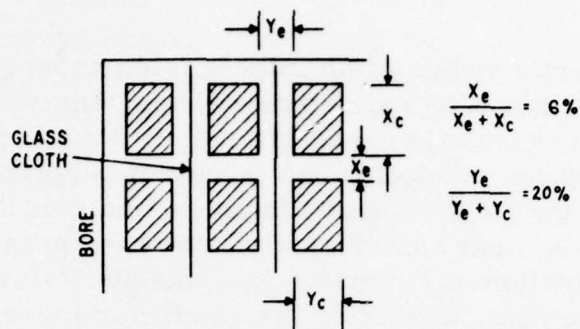


Figure 18. Conductor Spacing

The analysis described by Hust¹² was used to obtain approximate conductivities for the composite, assuming the spacing in Figure 18:

$$K_y = 0.0026 \text{ w/cm K}$$

$$K_x = 0.009 \text{ w/cm K}$$

RESULTS

As an example, a loss rate consistent with IGC conductor C was assumed. A General Electric two-dimensional, transient heat-transfer computer program was utilized to calculate the module temperature distribution during a one-second ramp. The field distribution in Section B (Figure 7) was assumed for this calculation and the losses were calculated by Equation--in Section VI.

Figure 19 is the temperature distribution in this section immediately following the ramp. The peak temperature, 8.5 K, is less than the 9 K critical temperature (listed in Table 9) for the peak field of 6.8 tesla at 20,000 A/cm².

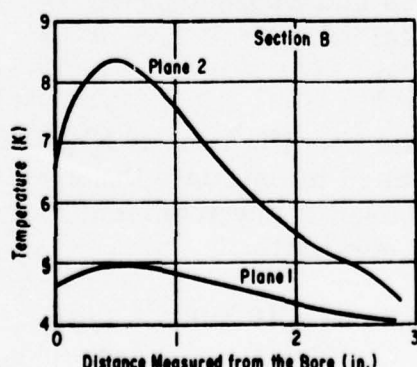


Figure 19. Temperature Distribution Following a One-Second Field Ramp

ASPECTED CONDUCTORS

The losses calculated with Equation 17(Section VI) for coefficients correlated to the loss values given in the survey responses apply only to fields parallel to the broad side of the aspected conductors. A correct analysis for an aspected conductor would include the effects of field orientation (Figure 20). Equation 19 attempts to account for the effects of field orientation on eddy current losses in aspected conductors: 13

$$\frac{Pe}{V} = \frac{\sigma_{\perp} |\bar{B}|^2}{4} \left\{ \left(\frac{L}{\pi} \right)^2 \left[\left(\frac{b}{a} \right)^2 \cos^2 \theta + \left(\frac{a}{b} \right)^2 \sin^2 \theta \right] + b^2 \cos^2 \theta + a^2 \sin^2 \theta \right\} \quad (19)$$

where: $\frac{Pe}{V}$ = loss per unit volume
 σ_{\perp} = effective anisotropic conductivity
 L = twist pitch
 $\frac{b}{a}$ = aspect ratio

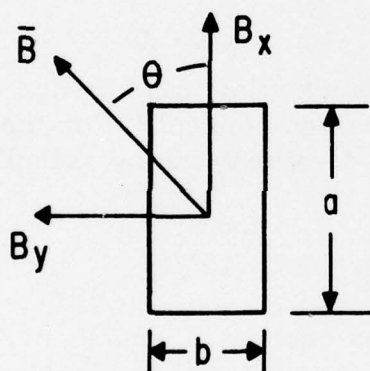


Figure 20. Field Orientation for an Aspected Conductor

The exact value of the exponent applied to the aspect ratio in this equation is somewhat in doubt, and the equation was derived for conductors less complex than the Nb_3Sn conductors proposed for this application. However, the equation does demonstrate a strong dependence on field orientation.

To compare the effects of normal and parallel fields for an aspected conductor, the ratio of the losses for fields in these directions can be calculated:

$$\frac{\frac{Pe}{V} (\theta = 90^\circ)}{\frac{Pe}{V} (\theta = 0^\circ)} = \frac{\left\{ \left(\frac{L}{\pi} \right)^2 \left(\frac{a^2}{b^2} \right) + a^2 \right\} B_y^2}{\left\{ \left(\frac{L}{\pi} \right)^2 \left(\frac{b^2}{a^2} \right) + b^2 \right\} B_x^2} \quad (20)$$

For IGC conductor C: $a = 0.103$ cm, $b = 0.023$ cm, and $L = 1.0$ cm.

Thus,

$$\frac{\frac{Pe}{V} (\theta = 90^\circ)}{\frac{Pe}{V} (\theta = 0^\circ)} = 402.2 \left(\frac{B_y}{B_x} \right)^2 \quad (21)$$

For the field distribution presented in Figure 10, the peak value of B_y is 3.27 tesla and the peak value of B_x is 6.8 tesla. The ratio of the losses associated with these fields is

$$\frac{\frac{Pe}{V} (\theta = 90^\circ)}{\frac{Pe}{V} (\theta = 0^\circ)} = 93.0 \quad (22)$$

The transient performance of a module utilizing a highly aspected conductor is determined primarily by the field acting normal to the conductor in this application. It can be concluded that the field orientation in the modules precludes the use of a highly aspected conductor.

RAMPING VOLTAGE

The voltage required to ramp the winding to design current in one second is inversely proportional to the design current. For the revised base design described in Table 5, the required voltage can be calculated by the following equation:

$$V = 6.23 \times 10^5 / I \quad (23)$$

A conductor with an operating current in excess of 300 amperes therefore requires 2 kV or less for the one-second ramp. A voltage of 2 kV is achievable with the epoxy-glass impregnation system.

Section VIII

QUENCH PROTECTION

INTRODUCTION

The operating current and copper cross sections are important considerations in the event of a quench. Temperature gradients in the module due to nonuniform dissipation of the winding stored energy can cause stressing and cracking of the winding module. This is particularly important in terms of winding tests when it may be desired to quench the winding. Normal zones in Nb₃Sn windings can be expected to propagate more slowly than those in NbTi windings, because of the higher heat capacity of the transition temperature.

SIMPLE PROTECTION CIRCUIT

The windings can be protected (at least during testing) by an external protection circuit. This circuit senses an asymmetrical voltage distribution in the winding and switches an external resistor in series with the winding. For large magnet systems the resistor is sized so that it determines the rate of current decay in the winding:

$$\tau = L/R = 2 \frac{E}{I_0 V_0} \quad (24)$$

$$I = I_0 e^{-t/\tau} \quad (25)$$

where: L = winding inductance

R = external resistance

I₀ = design current

V₀ = I₀R

E = winding energy = 3.113 × 10⁵ joules

The rate of decay is limited by the size of the external resistance. This must be limited to avoid an excessively high initial voltage, V₀.

To determine the internal temperature distribution following quench, the revised base design (Table 5) was assumed to have been manufactured with a 300-ampere conductor which is 40 percent copper. A transient heat-transfer computer program developed to investigate coil quenching was utilized. The field distribution was assumed initially to be that of Section B (Figure 7) and varied in proportion to the current.

It was assumed in the program that the external resistance (5.9 ohms) is not switched in series with the winding until 0.5 second after the initiation of the normal zone in a low-field corner of the module. The normal-zone voltage drop after 0.5 second was found to be 30 volts, which should be detectable even when superimposed on the ramping voltage.

Figure 21 is a temperature listing for the module cross section following dissipation of 95 percent of the stored energy. The temperature gradients are steep and the peak temperature is almost 180 K, indicating that the module would be severely stressed. The peak temperature can be reduced by increasing the size of the external resistor. The initial voltage when the 5.9 ohm resistor is switched in series with the winding is 1.75 kV.

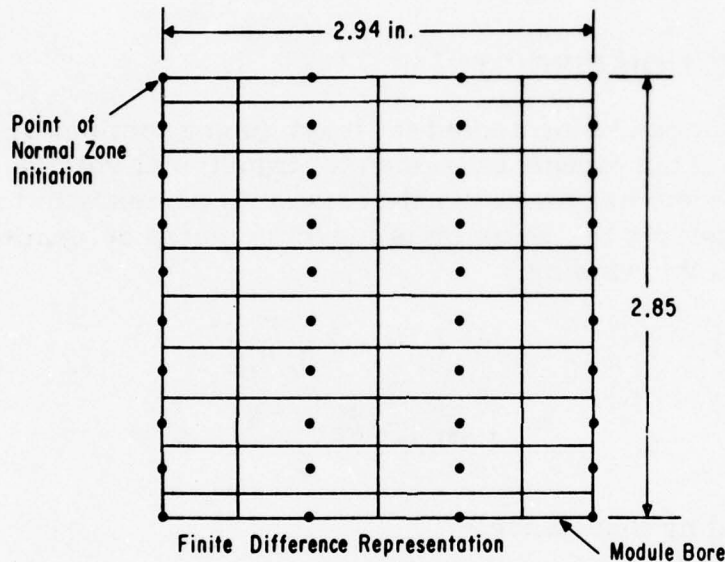


Figure 21. Nodal Representation and Module Temperature Distribution Following an Assumed Quench (with a Protection Circuit)

If the external resistance is increased to 11.8 ohms, the initial voltage will be 3.5 kV. The peak temperature following a quench similar to the previous example is 115 K. This temperature rise is more acceptable, but the high initial voltage places a substantial insulation requirement on the leads and winding.

The assumed quench is, in a sense, a worst case. The propagation of the normal zone from the point of initiation in the low-field region is slow as a result of the large temperature margin. Such a quench could only be initiated by wire motion in the module, module motion in the support, or a flaw in the superconductor.

The temperature rise to 115 K and the applied voltage of 3.5 kV are near the acceptable limits. Increasing the copper in the conductor will increase the transient losses. This indicates that 300 amperes is the lowest conductor current that results in a winding which can be adequately protected by the simple protection circuit.

ALTERNATE PROTECTION SYSTEMS

More complex protection circuits, which energize heaters on the surfaces of the modules to rapidly spread the normal zone throughout the winding, are possible; but the reliability of the protection circuit decreases with complexity. In addition, the previously discussed delay in the sensing of the normal zone results in a delay in the energizing of the heaters, diminishing the effectiveness of this protection scheme.

An alternate scheme could allow the use of lower current conductors. If the windings are wired in parallel (Figure 22) the conductor size can be reduced by a factor of 4 (75A).

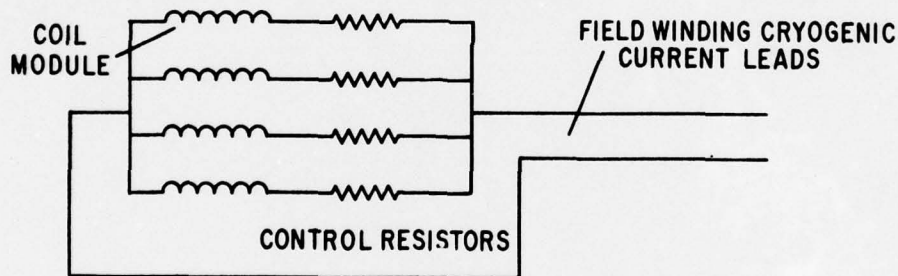


Figure 22. Parallel Module Winding

The connections are made in the winding region of the rotor to avoid the requirement for additional cryogenic current leads. To ensure equal currents immediately after ramping, this scheme requires that the modules be wound with nearly the same number of turns. Approximate analysis indicates that a 1 percent error in the number of turns in a module results in a 2 percent increase in the current carried by that module. This is an acceptable discrepancy in current for what is expected to be an achievable degree of winding symmetry.

If the winding is to be operated in a steady-state mode for extended periods of time, differences in joint resistance will result in unequal current sharing. This can be avoided by including control resistors in series with each module. The required resistors are large compared to expected joint resistances but

are small enough to result in acceptable levels of dissipation in the helium pool. For example, if a 75 ampere conductor is used with $10\ \mu\text{ohm}$ resistors, the steady-state dissipation in the four resistors is only 0.225 watt.

Section IX

ROTOR COMPONENT WEIGHTS AND SUPERCONDUCTOR PERFORMANCE

The generator dimensions will be optimized in Phase II for the selected superconductor characteristics, but the revised base design and the investigations of winding support and shielding systems have resulted in sufficient definition of the major rotor components to allow calculation of the weights of these components in the nonoptimized design. In addition, the effect on rotor weight of superconductor performance can be estimated.

Table 10 presents the component weights for rotors utilizing the support systems shown in Figures 16 and 17. In both designs the winding represents the largest component weight, and approximately two-thirds of the winding weight is in the 17.6 inch active length. The total of the major rotor component weights represents approximately one half of the design goal of 2000 pounds for the 20 MW generator (0.11b/kW).

Table 10

ROTOR COMPONENT WEIGHT ESTIMATES (Revised Base Design)

Component	Glass-Banded Torque Tube, Glass Filament Bore Tube (lb)	Steel Torque Tube Titanium Bore Tube (lb)
Winding	469.1	469.1
Torque Tube	89.5	210.5
Torque Tube Ext.	25.6	25.6
Radiation Shield	18.5	18.5
Electromagnetic Shield	53.9	53.9
Support Structure and Bore Tube	198.5	249.4
	<hr/> 855.1	<hr/> 1027.0

As was discussed in Section III, the field in the armature for the base design winding is approximately 70 percent of that in the annular-sector model of the sizing study. This resulted in an active length increase from 13.5 to 17.6 inches in the concentric-end-turn-machine. This represented a 30 percent increase in active length and approximately an 18 percent increase in the weight of the major rotor components. Similarly, an improvement in superconductor allowing a 1 percent increase in current and field would result in approximately a 0.6 percent decrease in rotor weight.

Section X

RECOMMENDED SUPERCONDUCTOR MEASUREMENTS

RECOMMENDED MEASUREMENTS

Table 11 presents the superconductor measurements that have been recommended. In the absence of experience with large modules, this information is important for the design of the rotor and the selection of a superconductor with characteristics required to meet the generator design goals. Of primary interest are the recommendations under the headings of losses, impregnation and insulation, current and field resistivity relations, and the effect of strain on resistivity. If these aspects of conductor performance are not experimentally verified, the rotor design will need to rely on engineering estimates.

Table 11

RECOMMENDED ADDITIONAL MEASUREMENTS OF Nb₃Sn PROPERTIES

<u>Priority</u>	<u>Description</u>
1	Losses The ramping losses as a function of the field angular orientation and magnitude (one-second ramp to fields of 1 to 8 tesla) are required for the design of a rotor with one-second ramping capability. The ac losses at 400 and 1200 hertz corresponding to negative sequence and the 5th and 7th harmonics of armature current from 0.1 to 10 gauss as a function of the angular orientation of the field are required for the design of an optimum electromagnetic shield configuration.
2	Mechanical Properties The elastic modulus as a function of direction of the conductor (and impregnated module) is required to determine the winding state of stress under various types of loading.
2	Thermal Properties The dimensional changes of the conductor (and module) during cooldown to 4 K are required for the design of the support structure and torque tube. The enthalpy of the conductor (and impregnated module) from 4 to 10 K is required to determine the ramping capability of the module. The conductor (and module) thermal conductance as a function of direction is of interest in considerations of transient and steady-state winding performance.
1	Impregnation and Insulation The application of polyvinyl formal insulation to Nb ₃ Sn conductors should be investigated. Impregnation of glass-wrapped conductors should be thoroughly investigated; penetration of the epoxy through the glass wrap must be demonstrated by cutting open an impregnated module and microscopically photographing the surface. The impregnation of cables should be investigated in a similar manner. The voltage capability of the insulation system should be investigated in high-pot tests.
1	Current Field Resistivity Relations Transient analysis indicates that 10 ⁻¹¹ ohm-cm approaches the tolerable limit for superconductor resistivity. Curves of resistivity are of interest in the region of 20,000 A/cm ² , 7 tesla, and 9 K as a function of field orientation.
1	Effect of Strain on Resistivity The effect of strain on resistivity in this region is also of interest both in consideration of bending and in consideration of centrifugal, thermal, and electromagnetic stressing of the module.
2	Propagation Velocity Since the field winding is high-energy-density device, the distribution of the energy following quench is of concern. In particular, the normal-zone propagation velocity in an adiabatic conductor as a function of field, current, and initial temperature could be measured and would provide a means for checking the analysis currently used to predict the temperature distribution following quench in an impregnated module.

CABLE IMPREGNATION

As discussed in Section VI, the impregnation of cables is a complex problem which can be verified only by the construction and testing of a coil module in a size comparable to that required by the base designs. Coil performance is a strong function of coil size. The successful impregnation of a large superconducting module requires that the winding be fully impregnated and may require that the superconductor be well bonded to the insulation, epoxy, or primer, depending on the details of the impregnation system. Small modules may perform successfully which utilize winding and impregnation techniques that prove unsatisfactory in large modules.

Figure 23 depicts a cylindrical module and a racetrack module. The volume of the cylindrical module is 10 percent of the volume of the four racetrack modules required in the base design. A cylindrical module could serve to verify the impregnation of the Nb_3Sn without requiring a complicated support structure. (The electromagnetic forces in a cylindrical module result in hoop stresses only).

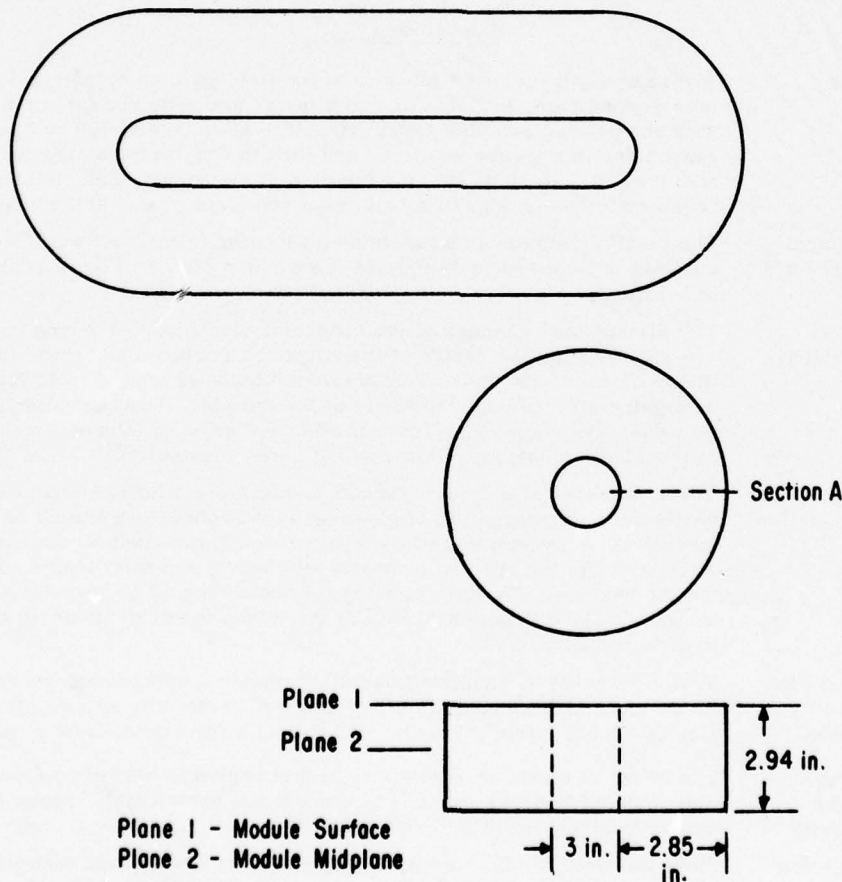


Figure 23. Cylindrical Module Geometry

The cylindrical-module field distribution has been investigated with a three-dimensional computer program for an assumed $15,000 \text{ A/cm}^2$ module current density. The results are plotted in Figure 24. The peak field is 12 percent higher than and the distribution is similar to that in the complete winding (Figure 7). Such a module could be used to verify the ramping capability of the superconductor in addition to verifying the impregnation of a cabled superconductor.

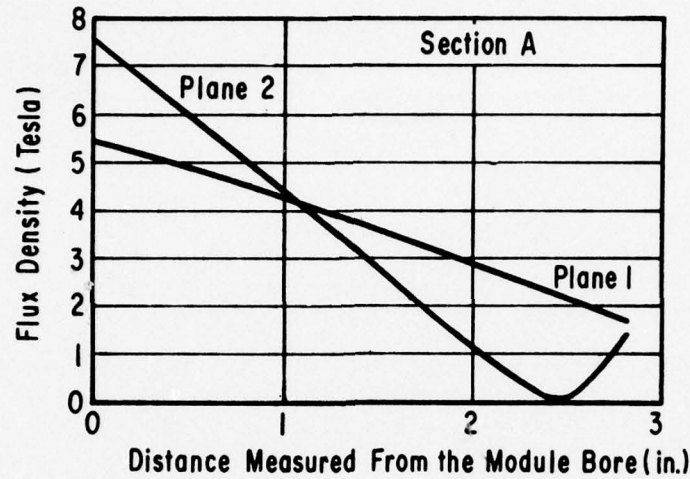


Figure 24. Cylindrical-Module Field Distribution

Assuming a conductor current density of $20,000 \text{ A/cm}^2$ and a packing factor of 75 percent, 4140 feet of 300 ampere conductor would be required to manufacture this cylindrical module. This is less than 10 percent of the superconductor required for the manufacture of the complete base-design winding.



Blank
58

Section XI

SUPERCONDUCTOR SELECTION

SUPERCONDUCTOR REQUIREMENTS

The analysis of the previous sections indicates a superconductor with the following characteristics is required for the revised base design with the modules connected in series:

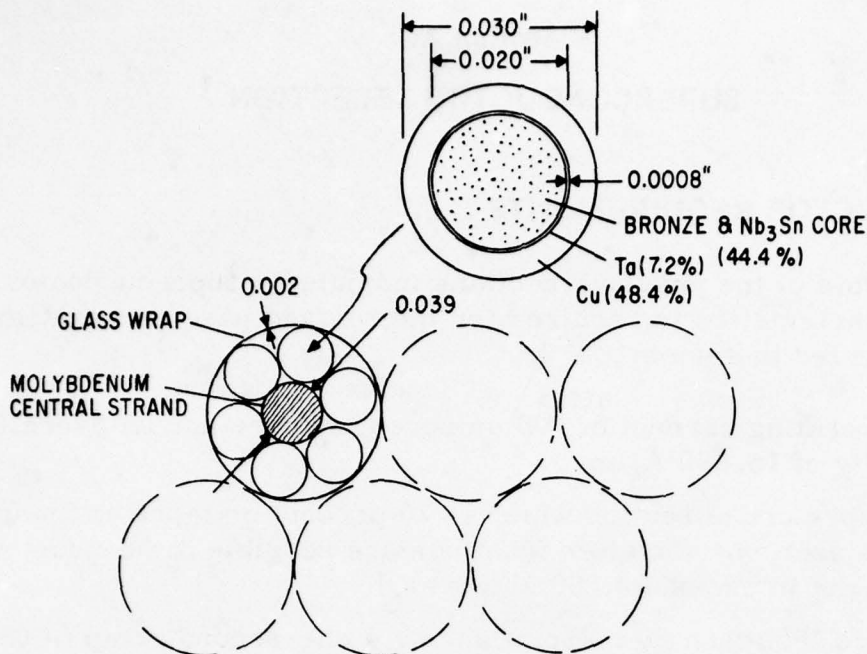
- An operating current of 300 amperes or more and an overall current density of 15,000 A/cm².
- A copper cross section which is 30 percent or more of the module cross section. (Smaller fractions are possible for conductors with currents in excess of 300 amperes.)
- Losses less than 60 mJ/cm² during a one-second ramp to 6.8 tesla.
- Ramping losses not strongly dependent on field orientation.
- A critical temperature of 8.5 K or more at the operating condition. (Lower critical temperatures are possible if the ramping losses are reduced.)
- Minimum bend radius less than 1.5 inches.

If the modules are connected in parallel, the current requirement is reduced to a minimum of 75 amperes.

PREFERRED CONDUCTOR SPECIFICATION

The results of the superconductor survey indicate a conductor of the desired size cannot be designed for the present application without aspecting or cabling. IGC indicated in their response to the survey that conductor D can be utilized in a cabled configuration consisting of six strands wrapped around a molybdenum central strand. IGC has also indicated this conductor can be scaled up 20 percent in diameter without deterioration of performance due to bending requirements.

Figure 25 is a schematic diagram of the preferred cable configuration. Cables necessarily result in a low packing factor; the resulting current density in the core is 7.11×10^4 A/cm² for the required module current density of 15,000 A/cm². The resulting operating current (864.6 amperes) is well in excess of the 300 amperes minimum required, allowing a reduced copper cross section (23 percent of the module cross section). The losses listed in Figure 25 were scaled from the values supplied in the survey for IGC conductor D.



BRONZE AND Nb₃Sn MODULE PACKING FACTOR = 0.211
 OVERALL CURRENT DENSITY = 15,000 A/cm²
 BRONZE AND Nb₃Sn CORE CURRENT DENSITY = 7.11 x 10⁴ A/cm²
 T_c = 8.4K (at 6.8 Tesla)
 = 9 K (at 6 Tesla)
 Cu FRACTION OF THE MODULE = 0.23
 CABLE CURRENT = 864.6 AMPERES
 LOSSES FOR A ONE SECOND RAMP TO 6.8 Tesla = 24.5 mJ/cm³ (in the strand)
 = 11.75 mJ/cm³ (in the module)

Figure 25. Preferred Cable Configuration

Figure 26 presents the current density in the core as a function of critical temperature at 6.8 tesla and 6 tesla. These curves are estimates obtained by scaling the current and field information supplied in the survey by IGC. The critical temperature corresponding to the desired operating point of 7.11×10^4 A/cm² in the core is 8.4 K at 6.8 tesla. The transient analysis of Section VIII indicated that the peak temperature following a ramp occurs at a point in the coil with a field of approximately 6 tesla. The critical temperature corresponding to the operating condition at 6 tesla is approximately 9 K.

The low transient losses and high current make this cable the preferred superconductor for the present application, but as has been discussed, the selection of a cable is necessarily contingent on successful impregnation and testing of a module of representative cross section. Such a module was described in Section X. The length of preferred conductor required for this cylindrical module is 1430 feet.

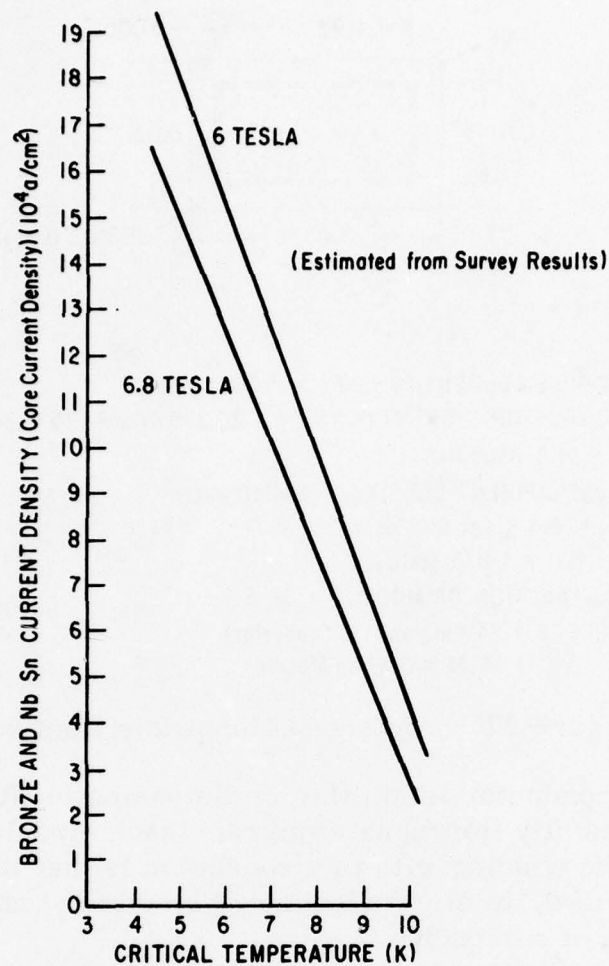


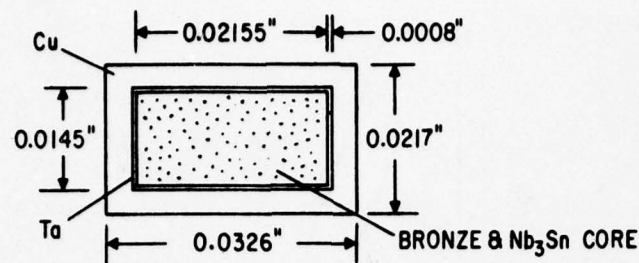
Figure 26. Core Current Density

PREFERRED MONOLITHIC CONDUCTOR SPECIFICATION

Should the impregnation of the preferred cabled configuration be less than fully successful, a lower-current monolithic conductor is preferred for use in a winding with the modules connected in parallel. The details of the parallel-module winding were discussed in Section IX.

The preferred monolithic conductor is schematically depicted in Figure 27. The conductor consists of one of the strands of the cabled configuration, formed in a rectangular configuration with a slight aspect ratio (1.5:1). The operating current listed in Figure 27 corresponds to an overall current density of 15,000 A/cm² and a conservative packing factor of 75 percent. The operating current corresponds to a critical temperature of 9.4 K at 6.8 tesla and 10 K at 6 tesla.

This conductor has low transient losses and a critical temperature well in excess of that required to achieve a one-second ramp to design current.



MODULE CURRENT DENSITY = 15,000 A/cm²
 CONDUCTOR CURRENT DENSITY = 20,000 A/cm² (75% packing)
 I = 91.2 AMPERES
 CORE CURRENT DENSITY = 45,050 A/cm²
 T_C = 9.4 K (at 6.8 Tesla)
 = 10 K (at 6 Tesla)
 Cu FRACTION OF MODULE = 36.3%
 LOSSES = 24.4 mJ/cm³ (in Conductor)
 = 18.36 mJ/cm³ (in Module)

Figure 27. Preferred Monolithic Configuration

This monolithic conductor is similar in dimension to NbTi conductors which have been successfully impregnated in racetrack modules. The disadvantage in constructing the winding with this conductor is that the modules must be connected in parallel, to allow adequate protection at an acceptable voltage level in the event of a quench.

The preferred cabled and monolithic conductors are compared in Table 12.

Table 12
PREFERRED CONDUCTORS

<u>Type</u>	<u>Pro</u>	<u>Con</u>
Cable	High current High specific heat Bend radius considerations divorced from conductor size and losses	Low packing factor Lower critical temperature Low thermal conductance Insulation and impregnation considerations
Monolithic	Good packing factor Good thermal conductance Higher critical temperature "Conventional" impregnation and insulation	Lower current Lower specific heat Parallel module considerations

Section XII

CONCLUSIONS

The sizing study resulted in the selection of preferred base designs which have the potential for meeting the weight requirements. Four-pole conductively shielded machines with involute and concentric armature end turns were selected for study. Four-pole machines are preferred because they exhibit competitive power density and are least sensitive to the approximations of the sizing study. Conductive shielding is preferred because of weight considerations; however, conductive shielding is ineffective when the rotor is at standstill. Therefore it is not practical to excite the field winding at standstill or low speed.

The work conducted in this phase has allowed the comparison of superconductors suggested for the present application by the superconductor manufacturers. There are several superconducting materials capable of meeting the superconductor requirements, but the preferred material, which is expected to be available within the time constraint of the present program, is Nb_3Sn .

The transient requirements dictate the winding configuration and the operating current density: The one-second spin-up requirement concurrent with field ramping necessitates the use of an epoxy-impregnated winding to avoid conductor motion under the sudden application of torsional, centrifugal, and electromagnetic loading. The operating current density is limited by the ramping rate. If the base designs were to be operated only in the steady state, the operating current density (and therefore the fields) could be increased by 35 percent above the selected value; this would decrease the required active length to generate 20 MW, and therefore would increase the power density. A weight penalty has been paid in the base designs to allow the desired ramping capability.

Much of the work conducted in this phase has consisted in analyzing the base designs to determine if support and shielding functions could be performed in the allotted space in the base designs. Several promising support configurations have been investigated to determine winding-to-support relative motion with sudden application of loading. The shielding investigation concluded that a thin aluminum shield would provide sufficient attenuation of ac fields, but that shield vibration is an important design consideration for generators with rectified load. It can be concluded that the base designs are a realistic vehicle for comparison of superconductor characteristics. These designs are far from complete and will be optimized in Phase II for the characteristics of the selected superconductor.

A preferred cable and a backup monolithic configuration have been discussed. The cable is preferred in that this configuration separates size, bend radius, and loss considerations, but either conductor results in a winding which has a strong

possibility of achieving the required one-second ramp rate while significantly advancing the state of the art of superconducting winding manufacture.

The preferred cabled superconductor configuration requires advancement of the state of the art. As part of the materials development program funded by the U.S. Air Force, cabled conductors will be developed capable of the needed bend radii to fabricate the generator field winding. The fabrication and test of a cylindrical coil of dimensions similar to the generator field winding is recommended as a means of reducing the technical risk for the construction of the rotor in Phase III.

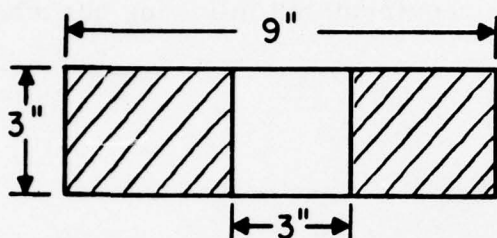
Appendix A
SUPERCONDUCTOR REQUIREMENTS

Appendix A

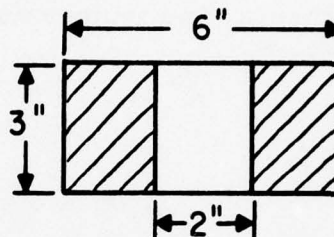
SUPERCONDUCTOR REQUIREMENTS

The requirements to be met in the selection of a superconductor can be described as follows:

- Volume of superconductor required: $1/3$ to 1 ft^3 (4 to 6 pieces)
- Winding configuration: potted racetrack modules are envisioned for use in an 18-inch-o. d. rotor. The modules will be held in a composite support structure. They will be immersed in a pool at approximately 4 K.



Module for four-pole machine
(4 required)



Module for six-pole machine
(6 required)

- Winding tension: 5,000 to 10,000 psi
- Insulation: 1 to 2 mils of polyvinyl formal
- Minimum bend radius: 1 to 1.5 inches
- Filament size and twist pitch: filament size must be selected to ensure adiabatic stabilization, and filament size and twist pitch must be selected in accordance with ramping loss requirements.
- Operating current: 400 to 1000 amperes
- Operating current density and ramping requirement: an operating superconductor current density of $20,000 \text{ A/cm}^2$ or greater is desired at 4 to 8 tesla peak field. The most severe operating requirement is that the winding be capable of a ramp to steady-state current in one second. This implies ramp rates of 4 to 8 T/sec for one second. The eddy and hysteresis losses in the superconductor can result in a substantial temperature rise in the potted module. The module surface is at 4 K, and preliminary analysis indicates that losses in the range of 20 to 40 mJ/cm^3 (of conductor) would result in 4 K temperature rise (depending on module design details). A desired superconductor would then have the following characteristics:
 1. $J_c > 20,000 \text{ A/cm}^2$ at 8 K and at least 4 tesla (possibly as high as 8 tesla).

2. Losses $< 40 \text{ mJ/cm}^3$ (a value as low as 20 mJ/cm^3 may be required) for a one-second ramp to a field of at least 4 tesla (possibly as high as 8 tesla).

This implies an A-15 superconductor, but alternate conductors are possible if the total ramping losses are substantially lower than the above values.

- Stabilization: preliminary analysis of the field winding after quench indicates that from 25 to 50 percent of the conductor cross section must be copper, to limit internal temperature gradients in the coil modules following a quench. The resistance ratio and the amount of copper will be selected consistent with stability, ramping requirements, and temperature gradient requirements following quench.

Appendix B
SUPERCONDUCTOR SURVEY

Table B. 1

CONDUCTOR A

Superconductor Manufacturer: Intermagnetics General Corporation

Superconductor Brand Name: Conductor A - Seven-strand cable with copper overwrap

Superconducting Material: Nb₃Sn

Configuration and Dimensions: Cable - six 0.0106" dia. bronze/Nb₃Sn/niobium composite strands cabled about a 0.013" dia. strengthening core, then overwrapped with six 0.007" dia. copper wraps. Circumscribed diameter of overall
Filament Diameter: 2μ
Number of Filaments: 6 x 4453 = 26, 718 cable: 0.0482 inch.

Twist Pitch: 5 to 10/inch in wire; 2 to 4/inch in cable

Stabilizer Resistivity Ratio: >150:1 (resistivity ratio in copper stabilizer)

Constituent Volume Fractions: Before Reaction: 43% Cu, 33% Bz, 24% Nb

Critical Current at 4 K and 6 K from 5 to 10 tesla: 220 A (10T, 2 K)*
~620 A (5T, 4.2 K)

Electrical Insulation: Glass overwrap

Manufacturing Dimensional Tolerances: ±0.0015 inch

Minimum Bend Radius: 0.64 inch (there is a 10% decrease in I_c at 0.5")

Cost/Ft³: to \$125, 000 to \$175, 000

Losses for 1 -second ramp from 0 to 4 tesla: 8 to 28 mJ/cm³ †

Losses for 1 -second ramp from 0 to 8 tesla: 28 to 100 mJ/cm³ †

*Critical current measurements listed are before heat treatment optimization. Measurements at 10 tesla, 4.2 K are approximately equivalent to 7 tesla, 8 K. For 4.0 K measurements, use ~10% higher than stated I_c values at 4.2 K.

† Depending upon solder resistivity and resistive cladding of the copper strands.

Table B. 2

CONDUCTOR A'
Under Development

Superconductor Manufacturer: Intermagnetics General Corporation

Superconductor Brand Name: Conductor A' - Seven-strand cable with copper overwrap

Superconducting Material: Nb₃Sn

Configuration and Dimensions: Cable: six 0.0212" diameter bronze/Nb₃Sn/Nb composite strands cabled about a 0.026" dia. strengthening core, then overwrapped with six 0.014" dia. copper wraps. Circumscribed diameter of overall
Filament Diameter: 2μ
Number of Filaments: 6 x 22, 862
= 137, 172
cable: 0.0964 inch.

Twist Pitch: 25 to 5/inch in wire, 1 to 2/inch in cable

Stabilizer Resistivity Ratio: >150:1 (resistivity ratio in copper stabilizer)

Constituent Volume Fractions: Before Reaction: 43% Cu, 33% Bz, 24% Nb

Critical Current at 4 K and 8 K from 5 to 10 tesla: 880 A (10 T, 4.2 K)*
2480 A (5 T, 4.2 K)

Electrical Insulation: Glass Overwrap

Manufacturing Dimensional Tolerances: ±0.0015 inch

Minimum Bend Radius: 1.3 inches

Cost/Ft³: \$125, 000 to \$175, 000

Losses for 1-second ramp from 0 to 4 tesla: 30 to 110 mJ/cm³ †

Losses for 1-second ramp from 0 to 8 tesla: 110 to 400 mJ/cm³ †

*Critical current measurements listed are before heat treatment optimization. Measurements at 10 tesla, 4.2 K are approximately equivalent to 7 tesla, 8 K. For 4.0 K measurements, use ~10% higher than stated I_c values at 4.2 K.

† Depending upon solder resistivity and resistive cladding of the copper strands.

Table B. 3

CONDUCTOR B

Superconductor Manufacturer: Intermagnetics General Corporation
Superconductor Brand Name: Conductor B - Copper laminated, aspected conductor
Superconducting Material: Nb₃Sn

Configuration and Dimensions: Rectangle/laminated
Overall conductor dimensions: 0.056 x 0.0278 in.²

Filament Diameter: ~4.5 μ

Number of Filaments: 4453

Twist Pitch: 2 to 4/inch

Stabilizer Resistivity Ratio: 150:1 (resistivity ratio in copper stabilizer)

Constituent Volume Fractions: Before Reaction: 68.5% Cu, 22% Bz, 9.5% Nb

Critical Current at 4 K and 8 K from 5 to 10 tesla: 90 A (10 T, 4.2 K)*
250 A (5 T, 4.2 K)

Electrical Insulation: Tape/Glass/Varnish

Manufacturing Dimensional Tolerances: ±0.0015 inch

Minimum Bend Radius: 0.5 inch

Cost/Ft³: \$100,000 to \$150,000

Losses for 1-second ramp from 0-4 tesla: 8 mJ/cm³ †

Losses for 1-second ramp from 0 to 8 tesla: 28 mJ/cm³ †

*Critical currents listed are before heat treatment optimization.
Measurements at 10 tesla, 4.2 K are approximately equivalent to 7 tesla, 8 K.
For 4.0 K measurements, use 10% higher than stated I_C values at 4.2 K.

† Assumes transverse field parallel to the wide side of the conductor.

Table B. 4

CONDUCTOR B'

Superconductor Manufacturer: Intermagnetics General Corporation
Superconductor Brand Name: Conductor B' - Copper-laminated, aspected conductor
Superconducting Material: Nb₃Sn
Configuration and Dimensions: Rectangular/Laminated
Overall conductor dimension: 0.112 x 0.0556 in²
Filament Diameter: ~4.5 μ
Number of Filaments: 22, 862
Twist Pitch: 1 to 2/inch
Stabilizer Resistivity Ratio: >150:1 (resistivity ratio in copper stabilizer)
Constituent Volume Fractions: Before Reaction: 68.5% Cu, 22% Bz, 9.5% Nb
Critical Current at 4 K and 8 K from 5 to 10 tesla: 400 A (10 T, 4.2 K)*
1100 A (5 T, 4.2 K)
Electrical Insulation: Tape/Glass/Varnish
Manufacturing Dimensional Tolerances: ±0.0015 inch
Minimum Bend Radius: 1.0 inch
Cost/Ft³: \$100, 00 to \$150, 000
Losses for 1-second ramp from 0-4 tesla: 32 mJ/cm³ †
Losses for 1-second ramp from 0 to 8 tesla: 110 mJ/cm³ †

*Critical currents listed are before heat treatment optimization.
Measurements at 10 tesla, 4.2 K are approximately equivalent to 7 tesla, 8 K.
For 4.0 K measurements, use 10% higher than stated I_c values at 4.2 K.

† Assumes transverse field parallel to the wide side of the conductor.

Table B. 5

CONDUCTOR C

Superconductor Manufacturer: Intermagnetics General Corporation
Superconductor Brand Name: Conductor C - Copper-clad monolith with subdivided integral copper
Superconducting Material: Nb₃Sn

Configuration and Dimensions: Aspected/monolith ~0.023 in. x 0.0103 in.

Filament Diameter: 3 μ

Number of Filaments: 142 x 161 = 22, 862

Twist Pitch: 2 to 3/inch

Stabilizer Resistivity Ratio: >100:1 (resistivity ratio in subdivided integral copper)

Constituent Volume Fractions: Before Reaction 40.5% Cu, 12.2% Ta, 34.5% Bz, 12.8 % Nb

Critical Current at 4 K and 8 K from 5 to 10 tesla: ~500 A (10 T, 4.2 K)*
1400 A (5 T, 4.2 K)

Electrical Insulation: Film/Glass/Tape

Manufacturing Dimensional Tolerances: ± 0.001 inch

Minimum Bend Radius: ~1.5 inches

Cost/Ft³: \$125, 000 to \$175, 000

Losses for 1-second ramp from 0 to 4 tesla: 22mJ/cm³†

Losses for 1-second ramp from 0 to 8 tesla: 78 mJ/cm³†

*Measurements at 10 tesla, 4.2 K are approximately equivalent to 7 tesla, 8 K.
For 4.0 K measurements, use ~10% higher than stated I_C values at 4.2 K.

† Assumes transverse field parallel to the west side of the conductor.

CONDUCTOR D

Superconductor Manufacturer: Intermagnetics General Corporation
Superconductor Brand Name: Conductor D - Copper-clad monolithic
Superconducting Material: Nb₃Sn

Configuration and Dimensions: 0.025" dia. bronze/Nb core separated from copper cladding by a tantalum barrier

Filament Diameter: 1.4 μ

Number of Filaments: 142 x 161 = 22,862

Twist Pitch: 4 to 6/inch

Stabilizer Resistivity Ratio: >100 (resistivity ratio in subdivided integral Cu)

Constituent Volume Fractions: Before Reaction: 45.5% Cu, 34.5% Bz, 7.2% Ta, 12.8% Nb

Critical Current at 4 K and 8 K from 5 to 10 tesla: 100 (10 T, 4.2 K)*
280 (5 T, 4.2 K)

Electrical Insulation: Wrap/Film

Manufacturing Dimensional Tolerances: 0.0005 inch

Minimum Bend Radius: (Expected) 0.85 inch

Cost/Ft³: \$125,000 to \$175,000

Losses for 1-second ramp from 0 to 4 tesla: 8 mJ/cm³

Losses for 1-second ramp from 0 to 8 tesla: 22 mJ/cm³

*Measurements at 10 tesla, 4.2 K are approximately equivalent to 7 tesla, 8 K.
For 4.0 K measurements, use ~10% higher than stated I_C values at 4.2 K.

NOTE: The conductor described is a base conductor element, which can be fabricated into a cable/braid, or Rutherford-type, construction.

Example: Seven-Strand Rutherford Cable (85% dense)

Diameter: ~0.045 in. x 0.114 in.

Minimum Bend: ~1.7 in. radius

Critical Current: 700 A (10 T, 4.2 K)

Table B. 7

CONDUCTOR E

Superconductor Manufacturer: Intermagnetics General Corporation
Superconductor Brand Name: CRYOSTRAND-Sn Cable (Conductor E)
Superconducting Material: Nb₃Sn

Configuration and Dimensions: Seven-strand cable - six superconducting strands 0.007" dia. cabled about a high-strength central core. Overall cable dimensions: 0.024 inch

Filament Diameter: ~6 μ

Number of Filaments: 222 x 6 = 1380

Twist Pitch: 1/3 inch in wire, 4 to 5/8 inch in cable

Stabilizer Resistivity Ratio: >100:1 (resistivity ratio in core copper)

Constituent Volume Fractions: Before Reaction: 10% Cu, 65% Bz, 25% Nb

Critical Current at 4 K and 8 K from 5 to 10 tesla: >180 A (10 T, 4.2 K)*
>450 A (5 T, 4.2 K)

Electrical Insulation: Glass Overwrap

Manufacturing Dimensional Tolerances: 0.0015 inch

Minimum Bend Radius: 0.8 inch

Cost/Ft³: \$90,000 to \$120,000

Losses for 1-second ramp from 0 to 4 tesla: 8 mJ/cm³

Losses for 1-second ramp from 0 to 8 tesla: 22 mJ/cm³

*Measurements at 10 tesla, 4.2 K are approximately equivalent to 7 tesla, 8 K.

For 4.0 K measurements, use ~10% higher than stated I_c values at 4.2 K.

NOTE: 6 CRYOSTRAND-Sn cables can be cabled about a central core to produce a conductor with a critical current of ~1080 A (10 T, 4.2 K) (see attached picture).

Table B.8

AIRCO CONDUCTOR A

Superconductor Manufacturer:	AIRCO, Inc.
Superconductor Brand Name:	(Conductor A)
Superconducting Material:	Monolithic multifilamentary Nb ₃ Sn
Configuration and Dimensions:	0.30 x 1.52 mm ²
Filament Diameter:	4.5 μm
Number of Filaments:	5377
Twist Pitch:	11 mm
Stabilizer Resistivity Ratio:	≥ 100
Constituent Volume Fractions: (before reaction)	18.1% Nb, 4.5% Ta, 25% Cu, 52.4% Bz
Critical Current at 4 K and 8 K from 5 to 10 tesla:	400 A at 8 K, 3.95 T
Electrical Insulation:	Special coating equipment must be developed
Manufacturing Dimensional Tolerances:	Standard
Minimum Bend Radius:	25 mm
Cost/Ft ³ :	Approx. \$62,500/ft ³ ; \$250/kg in quantities over 100 kg
Losses for 1-second ramp from 0 to 4 tesla:	-----
Losses for 1-second ramp from 0 to 8 tesla:	-----

Table B. 9

AIRCO CONDUCTOR B

Superconductor Manufacturer:	AIRCO, Inc.
Superconductor Brand Name:	(Conductor B)
Superconducting Material:	Monolithic multifilament Nb ₃ Sn
Configuration and Dimensions:	0. 46 x 2. 29 mm
Filament Diameter:	2. 4 μm
Number of Filaments:	37, 439
Twist Pitch:	17 mm
Stabilizer Resistivity Ratio:	≥ 100
Constituent Volume Fractions: (before reaction)	34% Cu, 4% Ta, 12. 9% Nb, 49% Br
Critical Current at 4 K and 8 K from 5 to 10 tesla:	400 A at 8 K, 6. 6 T
Electrical Insulation:	Special coating equipment must be developed
Manufacturing Dimensional Tolerances:	Standard
Minimum Bend Radius:	38 mm
Cost/Ft ³ :	Approx. \$75, 000/ft ³ ; \$300/kg in quantities over 100 kg
Losses for 1-second ramp from 0 to 4 tesla:	----
Losses for 1-second ramp from 0 to 8 tesla:	----

Table B. 10

AIRCO CONDUCTOR C

Superconductor Manufacturer:	AIRCO, Inc.
Superconductor Brand Name:	(Conductor C)
Superconducting Material:	Monolithic multifilament Nb ₃ Sn
Configuration and Dimensions:	0.46 x 1.83 mm
Filament Diameter:	4.6 μm
Number of Filaments:	6289
Twist Pitch:	12 mm
Stabilizer Resistivity Ratio:	≥ 100
Constituent Volume Fractions: (before reaction)	50% Cu, 10% Nb, 3% Ta, 37% Bz
Critical Current at 4 K and 8 K from 5 to 10 tesla:	400 A at 8 K, 4.7 T
Electrical Insulation:	Special coating equipment must be developed
Manufacturing Dimensional Tolerances:	Standard
Minimum Bend Radius:	38 mm
Cost/Ft ³ :	Approx. \$50,000/ft ³ ; \$200/kg in quantities over 100 kg
Losses for 1-second ramp from 0 to 4 tesla:	-----
Losses for 1-second ramp from 0 to 8 tesla:	-----

Table B.11

AIRCO CONDUCTOR D

Superconductor Manufacturer:	AIRCO, Inc.
Superconductor Brand Name:	(Conductor D)
Superconducting Material:	Multistrand multifilament Nb ₃ Sn
Configuration and Dimensions:	Flat cable or braid from 0.3 mm diameter strand with up to 100 strands
Filament Diameter:	3.5 μm
Number of Filaments:	1045 per strand
Twist Pitch:	~5 mm
Stabilizer Resistivity Ratio:	≥ 100
Constituent Volume Fractions: (before reaction)	30.6% Cu, 13.2% Ta, 14.5% Nb, 41.8% Bz
Critical Current at 4 K and 8 K from 5 to 10 tesla:	45 A/strand at 8 K, 4.7 T
Electrical Insulation:	To be developed
Manufacturing Dimensional Tolerances:	Standard
Minimum Bend Radius:	25 to 40 mm, depending on compaction
Cost/Ft ³ :	Approx. \$100,000/ft ³ ; \$400/kg in quantities over 100 kg
Losses for 1-second ramp from 0 to 4 tesla:	----
Losses for 1-second ramp from 0 to 8 tesla:	----

Table B. 12

SUPERCON

Superconductor Manufacturer:	Supercon, Inc.
Superconductor Brand Name:	Supercon
Superconducting Material:	NbTi and Nb ₃ Sn
Configuration and Dimensions:	Flat braid approx 0.3 in. x 0.030 in. , 65 strands, CuNi-clad strands 0.010 in. diameter
Filament Diameter:	9×10^{-6} m
Number of Filaments:	25,800
Twist Pitch:	3×10^{-3} m
Stabilizer Resistivity Ratio:	50 to 100 (H=0)
Constituent Volume Fractions:	Cu: SC = 1: 1
Critical Current at 4 K and 8 K from 5 to 10 tesla:	See below*
Electrical Insulation:	Wrapped or separate during coil winding
Manufacturing Dimensional Tolerances:	± 0.002 inch
Minimum Bend Radius:	1 inch for NbTi; 3 inches for Nb ₃ Sn
Cost/Ft ³ :	Approximately \$170,000 for Nb ₃ Sn or \$130,000 for NbTi
Losses for 1-second ramp from 0 to 4 tesla:	Est. 18 mJ/cm ³
Losses for 1-second ramp from 0 to 8 tesla:	Est. 62 mJ/cm ³
Losses based on Oak Ridge Laboratory criterion.	

*Critical current at 4 K only from

	<u>5</u>	<u>6</u>	<u>7</u>	<u>8</u>	<u>9</u>	<u>10</u> tesla
NbTi	2300	1880	1520	1130	650	325
Nb ₃ Sn	4000	3200	2300	1650	1170	800

Table B. 13
HISUPER 331; ZF-120B

Superconductor Manufacture:	Hitachi Ltd.
Superconductor Brand Name:	HISUPER 331 ZF-120B
Superconducting Material:	NbTiZr
Configuration and Dimensions:	Braided conductor 0.7 x 6.4 mm
Filament Diameter:	5 μ m
Number of Filaments:	331 x 120
Twist Pitch:	2 mm
Stabilizer Resistivity Ratio:	> 100
Constituent Volume Fractions:	17% NbTiZr, 30% Cu, 53% solder
Critical Current at 4 K, 5 T:	1710 A
4 K, 10 T:	117 A
8 K, 5 T:	0
8 K, 10 T:	0
Electrical Insulation:	Kapton 50 μ m
Manufacturing Dimensional Tolerances:	± 0.1 mm
Minimum Bend Radius:	15 mm
Cost/Ft ³ :	Approx. \$75,000
Losses for 1-second ramp (0 \rightarrow 4T)	3.1 mJ/cm ³
(0 \rightarrow 8T)	7.1 mJ/cm ³

Table B. 14

HISUPER 331; CF-96B

Superconductor Manufacture:	Hitachi Ltd.
Superconductor Brand Name:	HISUPER 331 CF-96B
Superconducting Material:	Nb ₃ Sn
Configuration and Dimensions:	Braided conductor 0.76 x 10 mm
Filament Diameter:	5 μm
Number of Filaments:	331 x 96
Twist Pitch:	2 mm
Stabilizer Resistivity Ratio:	> 100
Constituent Volume Fractions:	12% Nb + Nb ₃ Sn, 12% Cu, 18% Bz, 11% SUS, 47% solder
Critical Current at 4 K, 5 T:	1500 A
4 K, 10 T:	470 A
8 K, 5 T:	1000 A
8 K, 10 T:	260 A
Electrical Insulation:	Kapton 50 μm
Manufacturing Dimensional Tolerances:	± 0.1 mm
Minimum Bend Radius:	38 mm
Cost/Ft ³ :	Approx. \$94,000
Losses for 1-second ramp (0→4T)	1.5 mJ/cm ³
(0→8T)	3.4 mJ/cm ³

Table B. 15

TOSHIBA

Superconductor Manufacturer:	Toshiba
Superconductor Brand Name:	
Superconducting Material:	Nb ₃ Sn
Configuration and Dimensions:	Stranded cable, six 0.36 strands wound on tungsten or stainless steel reinforcement
Filament Diameter:	Outer diameter 19 microns Inner diameter 12 microns
Number of Filaments:	127 per strand
Twist Pitch:	10 to 20 mm
Stabilizer Resistivity Ratio:	150
Critical Current:	420 A at 4 T
Electrical Insulation:	Formal
Manufacturing Dimensional Tolerances:	0.01 mm
Minimum Bend Radius:	36 mm
Cost/Ft ³ :	\$128,000
Losses:	

bl
86

REFERENCES

1881

REFERENCES

1. Kirtley, J. L., Jr., "Armature of the MIT-EPRI Superconducting Generator," submitted to Power Engineering Society, Institute of Electrical and Electronics Engineers, New York, N. Y.
2. Kirtley, J. L. Jr., and Steeves, M. M., "Toroidal Winding Geometry for High-Voltage Superconducting Alternators," IEEE Transactions--Power Apparatus and Systems, Vol. PAS-93, No. 6, November/December 1974, pp. 1902-1908.
3. Say, M. G., Performance and Design of Alternating Current Machines, 3d ed., Pitman & Sons, Ltd., London, 1958, p. 213.
4. "Advanced Superconducting Rotor," Section 2, Technical Proposal to Aero Propulsion Laboratory, Wright-Patterson Air Force Base: General Electric Corporate Research and Development, Schenectady, N. Y., July 1976.
5. "Electromechanically Driven and Tuned Vibrations in Superconducting Alternators," Keim, T. A., Thullen, P., and Shevchuk, G. J., Paper No. A76-123.0, Institute of Electrical and Electronics Engineers, New York, N. Y.
6. Stuart, T. A., and Tripp, M. W., "Predicted Characteristics of the Superconducting Alternator with Rectified Load," National Aerospace Electronics Conference (IEEE), Dayton, Ohio, May 1977.
7. Walker, M. S. et al., Manufacturing Technology of Multifilamentary Nb₃S for Superconducting Rotor Coil Applications, Third Quarterly Report, December 1975 - February 1976, to Air Force Materials Laboratory, Wright-Patterson Air Force Base: Intermagnetics General Corporation, Guildersland, N. Y.
8. Shevchuk, G. J., "Mechanical Design of Electromagnetic Shields for Superconducting Rotors," PhD thesis, Massachusetts Institute of Technology, Cambridge, Mass., 1976.
9. Crow, J. E. and Suenaga, M., "The Temperature Dependence of Superconducting Critical Current Densities of Multifilamentary A-15 Composite Wires," Proceedings of the 1972 Applied Superconductivity Conference, Pub. No. 72CHO682-5-TABSC, Institute of Electrical and Electronics Engineers, New York, N. Y.
10. Vieland, L. J. and Wicklund, A. W., "Specific Heat of Niobium-Tin," Physical Review, Vol. 166, Feb. 1968, pp. 424-431.

11. Johnson, V. A. , A Compendium of the Properties of Materials at Low Temperatures (Phase 2), Part 1 Properties of Solids, WADD Tech Rept 60-56, Wright-Patterson Air Force Base, Ohio, October 1960.
12. Hust, J. G. , "Low Temperature Thermal Conductivity Measurements on Longitudinal and Transverse Sections of a Superconducting Coil, " Cryogenics, Vol. 15, January 1975, pp. 8-11.
13. Murphy, J. H. , Carr, W. J. , Walker, M. S. and Vecchio, P. P. , "Field Orientation Dependence of Losses in Rectangular Multifilamentary Superconductors, " Advances in Cryogenic Engineering, Vol 22, Plenum Press, New York, N. Y. , 1977, pp. 420-427.

END

DATE

FILMED

DTIC

July 88